Transplant immunosuppressant therapies induce unique functional changes in lymph node and re-shape gut immune homeostasis

Long Wu[1,2,+], Allison Kensiski[2,+], Samuel J Gavzy[1,2], Yang Song[3], Hnin Wai Lwin[3], Michael France[3,4], Dejun Kong[2], Lushen Li[1,2], Ram Lakhan[1,2], Vikas Saxena[1,2], Wenji Piao[1,2], Marina W. Shirkey[2], Valeria Mas[1], Brendan Lohmsr[1,2], Jonathan S Bromberg[1,2,4]*, Bing Ma[3,4]*

[1]University of Maryland School of Medicine, Department of Surgery, Baltimore, MD, USA

[2]University of Maryland School of Medicine, Center for Vascular and Inflammatory Diseases, Baltimore, MD, USA

[3]University of Maryland School of Medicine, Institute for Genome Sciences, Baltimore, MD, USA

[4]Department of Microbiology and Immunology, University of Maryland School of Medicine, Baltimore, MD, USA

[+]Authors contributed equally to this work

*Corresponding Authors:

Jonathan S. Bromberg, MD, PhD

jbromberg@som.umaryland.edu

Bing Ma, PhD

bma@som.umaryland.edu

Abstract

Current immunosuppressants effectively suppress adaptive and innate immune responses, but their broad, antigen-non-specific effects often result in significant complications. Here, we conducted a systematic investigation of drug effects on gut microbiome, metabolic pathways, lymphoid architecture and lymphocyte trafficking of four major immunosuppressants classes including tacrolimus, prednisone, mycophenolate mofetil (MMF), and Fingolimod (FTY). We show that immunosuppressants induced progressive alterations in the gut microbiome and metabolic pathways, where initial drug-specific effects converged by day 30 into a common dysbiotic state enriched in Muribaculaceae. Gut transcriptome analyses revealed minimal overlap in differentially expressed genes between early and late time points, indicating transient early effects and marked late-stage changes induced by these drugs. These microbiome and metabolic shifts were accompanied by time-dependent changes in lymph node (LN) organization and cellular composition, transitioning between pro-tolerogenic and pro-inflammatory states. Under alloantigen-stimulated conditions, MMF and FTY suppressed inflammation through dual regulation of regulatory T cells and LN remodeling, mediated through LN stromal cell-derived laminins. Together, our findings highlight previously underappreciated temporal dynamics in immunosuppressant mechanisms, linking immune tissue organization, gut microbiome and intestinal responses to long-term immunosuppression and metabolic complications in transplant patients.

Introduction

Prevention of solid organ transplant rejection necessitates lifelong, multimodal immunosuppression to dampen both adaptive and innate alloreactive immunity. Despite improved short-term outcomes, long-term graft survival remains suboptimal due to chronic rejection and a range of adverse events such as metabolic complications, infections, neoplasia, and organ-specific toxicities [1-8]. Current immunosuppressants target specific immune pathways but are limited by their antigen-non-specific nature, broadly suppressing the immune system and causing off-target effects that impact non-immune cells[9, 10]. This dilemma between necessary immunosuppression and its imprecise, system-wide effects represents a critical challenge for improving transplant outcomes.

A comprehensive understanding of the immune suppressant drug effects is crucial to optimize therapeutic regimens and minimize adverse events while maintaining effective prevention of graft rejection. While most mechanistic research on immunosuppressants has focused on their effects on T cells, B cells, and dendritic cells, there is limited understanding of how these drugs impact secondary lymphoid organs (SLOs), particularly lymph nodes (LNs), which are key regulators of local and systemic immunity, directing responses toward either immune tolerance or activation. The architecture of LNs is maintained by LN stromal cells (LNSCs) networks, including fibroblastic reticular cells (FRCs), lymphatic endothelial cells (LECs), and blood endothelial cells (BECs). These LNSCs are critical for regulating the positioning and interactions of lymphocytes with antigen-presenting cells like DCs through the coordinated action of chemokines,

cytokines and stromal fibers [11-13]. FRC-derived laminins, in particular, influence global immune states by regulating the balance between tolerance and immunity [14, 15]. Specifically, a high laminin α4:α5 ratio (La4:La5) within the T cell cortex of the LN cortical ridge (CR) and around high endothelial venules (HEVs) promotes a pro-tolerogenic environment, while a low La4:La5 fosters inflammation and immunity. Additionally, LN structure and FRC function can be disrupted during transplantation due to ischemia-reperfusion injury to the graft, leading to immunologic scarring, a persistent and pathologic alteration to this cellular network [16, 17]. Understanding how immunosuppressants affect these architectural elements of immunity is crucial for enhancing long-term allograft survival.

Apart from the effects on specific immune cell populations, immunosuppressive drugs significantly impact the gut microbiome composition and their functional output, influencing alloimmunity and graft survival [18-22]. Our group has demonstrated that gut microbiota modulates LN architecture through alterations in stromal fiber laminins [23-25], establishing a crucial link between the gut microbiome and LN structure and function. Further, we observed significant alterations in both gut microbiome composition and metabolic activities under tacrolimus-induced immunosuppression in both luminal and systemic measurements [26]. Our recent work on inhibiting the mammalian target of rapamycin (mTOR) revealed its broad effects on gut microbiome structure, metabolic functions, and intestinal host responses, including changes in LN architecture [27][28]. Other studies have shown diverse mechanisms by which immunosuppressants affect host-microbe interactions. For instance, methotrexate

inhibits the conserved dihydrofolate reductase pathway in both host and gut bacteria, leading to broad microbiome alterations [29], while other immunosuppressants modify the intestinal environment through changes in barrier permeability [30]. Importantly, these host-microbe interactions are multidirectional, in that microbiota can alter intestinal function and drug bioavailability [31, 32]. For example, mycophenolate mofetil (MMF) is metabolized to inactive glucuronidated mycophenolic acid (MPAG) via hepatic glucuronidation, and luminal bacteria expressing β-glucuronidase can reactivate the metabolized form MPAG back to active MPA, leading to increased concentrations of active luminal drug and colonic inflammation [33]. Given these complex interactions between immunosuppressants, gut microbiota, intestinal function, and immune cell populations, understanding their intricate relationships is crucial to decipher both therapeutic effects and unintended drug effects.

In this study, we systematically investigated the previously understudied effects of immunosuppressants on LN architecture, the distribution of lymphocyte and myeloid cell populations, and gut microbiome and metabolome. Four key classes of clinical immunosuppressants were included: TAC (tacrolimus) from calcineurin inhibitor category, PRED (prednisone) from glucocorticoid category, MMF from inosine monophosphate dehydrogenase (IMPDH) inhibitor category, and FTY720 (Fingolimod) from S1P receptor antagonist category. Dynamic temporal drug effects were observed, where moderate early changes progressed to substantial alterations in the gut microbiome and metabolism after prolonged treatment. By day 30, despite their distinct mechanisms of action, all drugs converged to induce a similar dysbiotic state in the gut

microbiome. This convergence, marked by enrichment of pathobionts Muribaculaceae, suggests a common mechanism linking long-term immunosuppression to metabolic complications in transplant patients. Further, early treatment induced pro-inflammatory changes in LN architecture and cellular composition, while long-term treatment resulted in anti-inflammatory effects. Notably, in alloantigen-stimulated conditions, MMF and FTY720 suppressed alloantigen-induced pro-inflammatory changes through dual regulation of Tregs and LN architecture. These findings demonstrate complex dynamics among immunosuppressants, microbiome changes, and immune tissue organization, providing new insight into mechanism of action of long-term immunosuppressant use.

Results

Immunosuppressant treatments affect gut microbiome composition and function

We treated groups of C57BL/6 mice daily with four immunosuppressants (TAC, PRED, MMF and FTY), respectively, using untreated mice as controls. We analyzed the gut microbiome at early (3 days), intermediate (7 days), and late (30 days) time points. We performed whole community metagenomic sequencing on intraluminal stool samples collected from the colon and utilized the comprehensive mouse gut metagenome catalogue (CMGM) [34] (**Supplemental Table 1A**) for taxonomic profiling and Human Microbiome Project Unified Metabolic Analysis Network (HUMAnN2) (v0.11.2) [35] (**Supplemental Table 1B**) to analyze microbial metabolic pathways.

To evaluate drug effect on the gut microbiome, we calculated Bray-Curtis pairwise distances for taxonomic composition, comparing drug-to-control deviations from the untreated state and drug-to-drug differences between treatments. In drug-to-control comparisons, the effects were variable during early treatment by day 3, with some drugs increasing and others decreasing relative to controls (**Figure 1A**). However, by day 30, all treatment groups showed profound and significant alterations in their gut microbiome profiles, suggesting a cumulative effect of sustained immune suppression. The pattern was evident in both taxonomic composition and functional pathway analyses, with the most substantial changes emerging after prolonged treatment (**Figure 1B**). Drug-to-drug comparison revealed a pattern of temporal progression. The differences between treatment groups initially increased from day 3 to day 7, suggesting distinct early drug-specific effects on gut microbial communities (**Figure 1A**). FTY demonstrated milder

effects compared to other drugs during this period. By day 30, these inter-drug differences were substantially reduced, indicating a convergence of the effect of long-term immunosuppressant drugs on gut microbiome composition. This convergence was observed in both taxonomic profiles and functional pathway abundances (**Figure 1B**), suggesting that despite their different mechanisms of action, these distinct drugs ultimately drive the gut microbiome toward a similar altered state. These findings were further validated through β-diversity analyses. Principal Component Analysis (PCA) revealed clear clustering of 30-day samples, distinct from earlier time points, regardless of the specific immunosuppressant used (**Figure 1C**). Canonical Correspondence Analysis (CCA) confirmed these observations, demonstrating significant correlations between treatment duration and microbiome composition, with maximal separation occurring at 30 days while day 3 and 7 samples showed minimal divergence from controls (**Supplemental Figures 1A and 1B**). The temporal convergence of microbiome alterations across different immunosuppressant drugs revealed shared downstream influences of these drugs on host-microbe interactions, despite their diverse initial effects.

To identify specific microbial signatures associated with immunosuppression, we identified differentially abundant bacterial species between treatment groups and controls at each time point (**Figure 1D**). No individual taxonomic group showed consistent alterations across any time point in any treatment group. During early (day 3) and intermediate (day 7) time points, we observed sporadic alterations in various bacterial taxa, but these changes were transient and not maintained through the late

time point (day 30). By day 30, all treatment groups, despite their distinct mechanisms of action, converged on a common set of bacterial taxa that were not significant at the earlier time points. These taxa belonged exclusively to the family of Muribaculaceae (formerly known as S24-7), a predominant commensal group in the mouse gut microbiome, including *Duncaniella*, *Paramuribaculum intestinale*, and CAG-873, pathobionts that are both necessary and sufficient to induce diabetes [36]. Together, the data reveal time-dependent pattern of immunosuppressant effects. The convergent enrichment of pathobionts suggests that prolonged immunosuppression promotes a dysbiotic state that may contribute to the metabolic complications commonly observed in transplant patients.

<u>Immunosuppressants induce drug-specific alterations in gut metabolic profiles</u>

We next examined gut luminal metabolism at day 7, a timepoint our previous work identified as capturing rapid metabolic changes that precede microbiome alterations [26], indicating direct effects on both host and microbial metabolism. Using untargeted metabolomic assessment through capillary electrophoresis-mass spectrometry (CE/MS), we identified 264 distinct metabolites in the gut lumen after quality assessment (**Supplemental Table 2A-B**). Partial Least Squares Discriminant Analysis (PLS-DA) demonstrated clear separations of metabolic profiles among the different immunosuppressant treatments (**Supplemental Figure 2A**) with distinct top contributing metabolites for each group (**Supplemental Figure 2B)**. Hierarchical clustering heatmaps also showed distinct drug induced patterns of differentially abundant compounds (**Supplemental Figure 2C**), indicating the distinct drug-specific metabolic profiles in gut lumen after immune suppressant treatment.

Pairwise comparison of individual drugs to the no-treatment control, combined with enrichment analyses, revealed both shared and drug-specific effects on metabolic activities (**Table 1**, **Supplemental Table 2C-F**). TAC exhibited the most balanced metabolic impact, showing both significant increases and decreases across multiple pathways (**Figure 2A, Supplemental Table 2F**). TAC treatment led to marked increases in three major categories of metabolites: 1) elevated levels of multiple amino acids and their derivatives, indicating alterations in protein catabolism and/or amino acid utilization in both host and microbiome. 2) TAC enhanced pyrimidine metabolism suggesting increased nucleotide turnover. 3) Elevated sugars and sugar phosphates indicate enhanced glycolytic pathway activity and altered central carbon metabolism. TAC treatment also significantly decreased several key metabolic pathways. These included reduced levels of polyamines and their derivatives, biogenic amines, short-chain fatty acids (SCFAs), betaine, trimethylamine (TMA), and various organic acids.

PRED, MMF, and FTY demonstrated predominantly suppressive impacts on gut metabolism, with distinct patterns and scope. PRED exerted the most broad and profound suppressive effect, decreasing three to four times more compounds than other treatments while showing minimal metabolite increases (**Figure 2B, Supplemental Table 2D**). A broad spectrum of metabolites across multiple pathways were reduced, including amino acid derivatives, SCFAs, other microbial-derived metabolites like TMA, pyrimidine components, and polyamines. This suppressive pattern aligns with known widespread effects of PRED on cellular metabolism.

MMF showed a predominant suppressive effect but with more selective targeting of specific pathways (**Figure 2C, Supplemental Table 2E**). Key suppressed pathways include glyoxylate and dicarboxylate metabolism involved in the TCA cycle, branched-chain amino acids (BCAAs), tyrosine metabolism, and purine metabolism. MMF increased adenosine while reducing uric acid, consistent with its mechanism as an IMPDH inhibitor. This may reflect increased IMP availability leading to enhanced flux through adenosine pathways, directly linking metabolic changes to the MMF therapeutic mechanism. On the other hand, FTY demonstrated a moderate suppressive effect **Figure 2D, Supplemental Table 2C**). FTY increased nucleoside levels while decreasing nucleotides and SCFAs. It reduced arginine availability while increasing N^1,N^8-diacetylspermidine and spermidine, indicating a directed metabolic processed. In summary, these results demonstrate distinct drug-specific metabolic signatures in the gut environment: TAC's balanced modulatory effects across multiple pathways, PRED's broad and profound suppression, MMF's selective suppressive effect, and FTY's moderate changes focused on nucleotide metabolism. These data indicate that the significant metabolic alterations may contribute to both therapeutic effects and side effects of different immunosuppressive strategies.

<u>Immunosuppressants elicit time-dependent, drug-specific intestinal responses</u>

To investigate the reciprocal interactions between the altered gut microbiome and gut epithelium responses under drug treatment, we analyzed the intestinal transcriptome. Days 7 and 30 were chosen as they corresponded to the major gut microbiota alterations during drug treatments. Differentially expressed genes (DEGs) were

identified by comparing each drug group to the no-treatment control (**Supplemental Table 3A**). Analysis of DEGs showed that 30-day treatment altered 1.3 to 2 times more genes than 7-day treatment, with the majority showing decreased expression levels. This pattern suggests prolonged immunosuppression leads to more extensive transcriptional modulation in intestinal tissue. The magnitude of response elicited by each individual drug was distinct (**Figure 3A, Supplemental Table 3B**). At day 7, FTY resulted in the largest number of DEGs. By day 30, both FTY and PRED elicited stronger effects in terms of upregulation and downregulation of DEGs. TAC showed the most unbalanced response, with twice as many genes showing increased expression compared to decreased expression. In contrast, PRED and MMF treatments produced more balanced alterations in gene expression patterns, with a greater proportion of genes showing decreased expression levels at day 30 compared to day 7. This temporal shift indicates that prolonged treatment leads to broader changes in intestinal gene expression.

We used UpSet plots to analyze overlapping DEGs between days 7 and 30 and across different treatments. These plots revealed minimal shared genes between timepoints and across different immunosuppressants (**Supplemental Figure 3A-D, Supplemental Table 3C-F**). For instance, following PRED treatment, only 31 genes (15 upregulated, 16 downregulated) are consistently modulated at both timepoints; there are 255 genes uniquely regulated at day 7 (81 upregulated, 78 downregulated) and 371 genes uniquely modulated at day 30 (174 upregulated, 197 downregulated). This pattern holds true for all four drug treatments. The limited overlap in DEGs between the two

timepoints suggests these immunosuppressants induced distinct responses at day 7 and 30. Further, the drug impact is more pronounced at day 30 with greater number of DEGs at either up- or down-regulation, indicating that long-term immunosuppression involves increasingly distinct cellular processes for each drug. Analysis of DEG between treatment groups revealed that while these immunosuppressants shared some common regulatory targets, they predominantly acted through distinct patterns of gene expression (**Supplemental Figure 4A-B, Supplemental Table 3F-G**). The limited overlap in regulated genes, typically less than 20% between any two drugs and less than 5% across all four drugs, suggests highly drug-specific mechanisms of action. The findings further support that despite their common therapeutic goals, these immunosuppressants achieve immune modulation through largely independent molecular regulation in intestine.

To characterize intestinal immune responses, we combined RNA-seq pathway analysis with immunohistochemical (IHC) assessment of key immune populations. This approach allowed us to examine both broad transcriptional changes and specific alterations in CD11c+ dendritic cells (DCs) and Foxp3+ regulatory T cells (Tregs), two cell types critical for immune homeostasis. GO ontology analyses of immune-related pathways in DEGs revealed distinct temporal patterns among the four drugs (**Figure 3B**). At day 7, FTY decreased expression of genes involved in mucosal and humoral immunity, while other drugs showed moderate effects on B cell-mediated response pathways. By day 30, the pattern shifted dramatically: FTY increased expression across multiple immune pathways; MMF switched from early activation to broad reduction in

innate immune pathway expression; TAC progressed from moderate increases in lymphocyte and immunoglobulin pathways to stronger activation of both innate immunity and antibody production; and PRED maintained relatively modest effects on immune pathway expression throughout the treatment period. IHC analysis revealed that the drug effects were similarly time-dependent but transient (**Supplemental Figure 5A-C)**. For intestinal CD11c+ DCs, all four drugs decrease these at day 7 but had no effects on days 3 or 30. For intestinal Foxp3+ Tregs, there were some increases on day 3 (by TAC and FTY), some decreases on day 7 (by TAC, PRED, and FTY), and no effects by day 30. Together, these findings demonstrate that immunosuppressants induce complex time-dependent changes in intestinal immune responses, with each drug showing distinct patterns of gene expression and immune cell modulation that evolve over the course of treatment.

<u>Time-dependent impact of immunosuppressants on mesenteric and peripheral lymph nodes (mLN and pLN) organization</u>

We next investigated how immunosuppressants affected LN organization in both mucosal and systemic compartments by examining mLN and pLN, the primary draining sites for mucosal and systemic immunity, respectively. Using flow cytometry and IHC, we analyzed changes in the numbers and distribution of immune cell populations (B220+ B cells, CD4+ T cells, CD8+ T cells, Foxp3+ Tregs) and structural features La4:La5 in LNs. We particularly assessed the distribution of La4:La5 and Tregs in the CR and around the HEV of LNs to understand how immunosuppressants modulated cellular and structural aspects of immune organization.

In mLN, flow cytometry revealed that B cells, CD4+ T cells, CD8+ T cells and Foxp3+ Tregs were unaffected by TAC or MMF treatment at days 3, 7, or 30 (**Figure 4C**). In contrast, PRED treatment significantly reduced CD4+ T cells and B220+ B cells by day 30, with no significant changes at earlier time points (**Figure 4A, C**). FTY treatment increased Foxp3+ Tregs by day 30, with no changes at days 3 or 7 (**Figure 4B, C**). Overall, while CD8+ T cell populations remained not significantly changed across all conditions (data not shown), other populations showed treatment-specific changes that were only pronounced after prolonged use. IHC results revealed two patterns of changes. On one hand, after TAC or PRED treatment, no significant changes in Treg distribution were observed in the mLNs at any time points (**Figure 4D, E, H, I, Supplemental Figure 6A, B**). However, both drugs reduced the La4:La5 around the CR after 7 days (**Figure 4F, H, I, Supplemental Figure 6C**) and TAC also reduce it in the HEV after 7 days (**Figure 4G-I, Supplemental Figure 6D**). On the other hand, MMF and FTY showed similar patterns with an increased Treg distribution in the CR by day 7 followed by a decrease by day 30 (**Figure 4D, H, I, Supplemental Figure 6A**). They also decreased La4:La5 in both the CR and HEV (**Figure 4F-I, Supplemental Figure 6C, D**). The responses at day 3 were mixed, indicating unstable early reactions that converged in later time points after prolonged drug treatment. Overall these data indicate that despite their distinct mechanisms of action, all four immunosuppressants converge on promoting a more pro-inflammatory environment in mLN by day 30, characterized by reduced Treg presence and/or decreased La4:La5. Transitional changes began around day 7, with early changes at day 3 being variable. This dynamic

pattern suggests that prolonged immunosuppression may paradoxically create localized pro-inflammatory conditions in mucosal lymphoid tissues.

In pLN, distinct temporal patterns of immune cell modulation were observed. TAC and PRED had minimal effects on cellular composition (**Figure 5D**), while MMF selectively reduced CD4+ T cells by day 30 (**Figure 5A, D**). FTY showed the most dynamic changes: increasing B220+ B cells while decreasing CD4+ T cells at day 7 (**Figure 5B**), followed by elevated Foxp3+ Tregs and decreased CD4+ T cells by day 30 (**Figure 5C, D**). IHC analysis revealed drug-specific effects on both cellular distribution and structural features. TAC showed transient effects, increasing Treg distribution in the CR at day 7 (**Figure 5E, I, Supplemental Figure 7A, B**) without affecting laminin ratios (**Figure 5G-J, Supplemental Figure 7C, D**). PRED demonstrated only early structural changes by day 3 and only increases La4:La5 **(Figure 5E-J, Supplemental Figure 7A-D)**. MMF showed the most consistent anti-inflammatory profile, maintaining increased Treg distribution **(Figure 5E, F, I, J, Supplemental Figure 7A, B)** throughout the treatment period and increasing La4:La5 at day 3 **(Figure 5G-J, Supplemental Figure 7C, D)**. FTY showed only early anti-inflammatory effects, increasing both Treg distribution and La4:La5 at day 3 but not the later time points **(Figure 5E-J, Supplemental Figure 7A-D)**. Overall, these data reveal that immunosuppressants predominantly promote an anti-inflammatory state in pLN, characterized by increased Tregs and/or elevated La4:La5, particularly during early treatment phases.

MMF and FTY720 counteract alloantigen-induced pro-inflammatory changes through dual regulation of Tregs and LN architecture

Given the significant impact noted above of MMF and FTY on LN architecture with increasing Tregs and La4:La5 under homeostatic conditions (**Figure 4H, I, 5I, J**), we investigated their effects in an inflammatory context using allogeneic stimulation. Mice received allogeneic splenocytes (10^7 cells intravenously) with or without drug treatment, and responses were assessed after three days. While allogeneic cells alone did not affect Treg distribution in mLN or pLN (**Figure 6A, C**), the combination of drugs with allogeneic cells showed significant effects: MMF increased Tregs around mLN HEV, while FTY increased Treg in both mLN and pLN HEV and CR (**Figure 6A, C, E, F**). Allogeneic stimulation alone decreased La4:La5 in both pLN and mLN (**Figure 6B, D**), indicating a pro-inflammatory LN structural shift in the context of alloantigen-induced immune responses, consistent with our previous findings [15]. Both MMF and FTY treatments prevented this decrease, maintaining La4:La5 comparable to untreated controls **(Figure 6B, D, E, F)**. These findings demonstrate that MMF and FTY inhibit alloantigen-induced proinflammatory changes in LN organization through two complementary mechanisms: increasing Tregs and preserving tolerogenic laminin stromal architecture. This dual action on both T cell and stromal cell structural features suggests these drugs may be particularly effective at promoting a tolerogenic environment during allostimulation.

MMF and FTY effects are mediated through FRC derived laminins α4 and α5

Given the significant impact of MMF and FTY on LN architecture by affecting La4:La5 and the crucial role of FRC in laminin expression [14, 37], we investigated whether the

effects of these drugs on LNs are mediated through FRC-derived laminins. We utilized two laminin KO mouse strains: FRC-specific laminin α4 knockout (FRC-Lama4-KO; Pdgfrb-Cre+/- × Lama4$^{fl/fl}$) and FRC-specific laminin α5 knockout (FRC-Lama5-KO; Pdgfrb-Cre+/- × Lama5$^{fl/fl}$) mice. These models allowed us to specifically examine the role of FRC-derived laminin α4 and α5 in immunosuppressant-mediated effects on LN stromal organization.

In mLN, as noted above, 3-day treatment of WT mice with MMF or FTY did not affect laminin ratios in the mLNs (**Figure 4F-I, Supplemental Figure 6C, D**). MMF and FTY also did not affect laminin ratios in FRC-Lama4-KO mice (**Figure 7A-C, G**). However, in FRC-Lama5-KO mice, both drugs decreased the La4:La5 in CR of mLNs (**Figure 8D-G**). These results suggested that MMF and FTY effects on laminin composition is dependent on laminin α5 expression, indicating its critical role in maintaining the laminin balance in the mLN.

In pLNs, as noted above, 3-day treatment of WT mice with MMF or FTY each increased La4:La5 in the pLNs (**Figure 5G-J, Supplemental Figure 7C, D**). MMF also increased La4:La5 in both CR and HEV of FRC-Lama5-KO mice (**Figure 8D-G**), but not in FRC-Lama4-KO mice (**Figure 8A-C, G**). In contrast, FTY decreased La4:La5 in CR of FRC-Lama4-KO mice (**Figure 8A-C, G**) but not in FRC-Lama5-KO mice (**Figure 8D-G**). These findings indicated that MMF and FTY modulated La4:La5 through distinct mechanisms that depended on the presence of laminins α4 and α5 from FRCs, although the precise pathways involved remain to be determined.

Discussion

This study provides an in-depth characterization of the previously underappreciated complex interplay of immunosuppressants with the gut microbiome and metabolism, intestinal gene expression, mesenteric and peripheral LN organization, and lymphocyte trafficking over time. We observed prolonged immunosuppressant treatment leads to a convergent dysbiotic state in the gut microbiome by day 30, despite distinct drug-specific effects observed at earlier time points. This incremental drug effect suggests a common underlying mechanism related to immune suppression, rather than individual drug effects, that impacts gut microbial communities. In the context of the metabolic and intestinal response results, the influence on gut microbiome likely related to nutrient availability, immune modulation, and altered gut function, which favors a particular microbial community structure. Particularly notable is the consistent enrichment of Muribaculaceae family members by day 30, known mediators of metabolic disorders such as diabetes [36], suggesting a potential mechanistic link between long-term immunosuppression and metabolic complications commonly observed in transplant patients [38-40].

Each immunosuppressant exhibited distinct metabolic signatures that revealed both expected and unexpected mechanisms of action. TAC broadly alters amino acid metabolism and other microbial-derived metabolites such as SCFAs, suggesting an influence on gut microbiome. Previous studies reported gastrointestinal side effects like diarrhea and nonspecific abdominal discomfort after tacrolimus use [41]. PRED exerted a broad suppressive effect on metabolism, consistent with its known ability to inhibit

cellular functions and pro-inflammatory cytokines [42]. This reduction in amino acid derivatives, SCFAs, and polyamines provides insights into its metabolic side effects, including diabetes and osteoporosis [43-45]. The reduction in microbial-derived metabolites such, as TMA and SCFAs, suggests substantial disruption of host-microbe interactions. MMF selectively targeted specific metabolic pathways, revealing a more precise mechanism compared to PRED and TAC. Its effects on purine metabolism directly align with its known IMPDH inhibition. The impact on the TCA cycle and BCAA metabolism might explain its distinct side effect profile of gastrointestinal toxicity and inflammation [46, 47]. Previous studies report that by inhibiting the TCA cycle, MMF reduces ATP production in intestinal epithelial cells, impairing barrier integrity through disrupted tight junction protein assembly [30]. Its disruption of BCAA metabolism compromises enterocyte protein synthesis and repair, leading to increased enterocyte apoptosis and villous atrophy [48]. FTY showed the most moderate metabolic effects, focused primarily on nucleotide metabolism and specific amino acid pathways. The moderate suppressive effect with maintenance of other metabolic pathways might explain its generally better tolerability. These distinct metabolic signatures among drugs could influence nutrient availability, signaling molecules, and microbial substrates, thereby shaping separate ecological niches within the gut[49].

Notably, all drugs affected SCFA levels to some degree, suggesting a common impact on microbiota-dependent metabolic functions. This shared effect may contribute to the convergent microbiome changes observed by day 30 and could represent a fundamental mechanism underlying long-term immunosuppression. Reduction in SCFA-

producing bacteria can disrupt metabolic processes, influencing blood pressure regulation, lipogenesis, and blood glucose control [50]. It was shown that probiotic administration could reverse gut dysbiosis, particularly catabolic microbial profiles that involve sucrose and starch degradation [50]. Other studies have shown that probiotics can improve tacrolimus-induced gut dysbiosis, SCFA depletion, and hypertension by restoring the vascular redox state and improving endothelial nitric oxide synthase (eNOS) function [51, 52]. Differences in how these drugs alter amino acid metabolism suggest they exert distinct influences on protein synthesis and cellular energy balance, potentially explaining their varying effects on different immune cell populations. Arginine metabolism is particularly relevant, as it affects eNOS activity through the arginine-NO pathway, influencing NO production and reactive oxygen species (ROS) generation. These changes can impair endothelial function and modulate immune cell activation. We show that TAC and mTOR inhibitors like rapamycin drastically affect amino acid regulation [REF], including arginine metabolism, and both have documented vascular complications [53-55]. Research in restoring drug induced metabolic and microbial dysregulation is still at very early stages, and our findings emphasize the importance to mitigate the unintended effects on the gut microbiome and metabolism. They also support the value of metabolic profiling and longitudinal monitoring to inform personalized treatment strategies.

The gut serves as a critical interface connecting immunity to environmental stimuli, making its regulation essential for maintaining transplant tolerance [56-58]. Our findings indicate that immunosuppressants exert complex, time-dependent effects on the gut

environment, influencing immune responses, metabolic activities, and microbial communities. While the gut microbiome converged toward a common dysbiotic state by day 30, intestinal gene expression patterns became increasingly drug-specific, with minimal overlap in differentially expressed genes (<5% across drugs). The progressive divergence in gene expression profiles by day 30 indicated increasingly specialized cellular processes unique to each drug. This result means that even as microbial communities arrived at a similar configuration, the gut tissue itself continued to respond in uniquely tailored ways to each immunosuppressant. Such tissue-specific transcriptomic divergence likely reflects the direct drug actions on host cells, the host's compensatory adjustments, and bidirectional interactions with microbiome metabolism. Understanding these complex interplays emphasizes the need for monitoring and potentially mitigating these effects in clinical practice.

Our study reveals the anatomically distinct and temporally dynamic effects of immunosuppressants on lymphoid tissue organization. One key observation is the divergent effect between mucosal and peripheral LN compartments. The pLN maintained an anti-inflammatory state, characterized as elevated Tregs and La4:La5, especially during early treatment phases. The pLN response aligns with the intended immunosuppressive effects of these drugs. On the other hand, in mLNs, which drain the intestine, all four drugs ultimately promoted a pro-inflammatory environment, characterized by reduced Tregs and decreased La4:La5. This compartment-specific regulatory effect may suggest a potential mechanism for some gastrointestinal side effects seen with immunosuppression [26].

The crucial role of FRC-derived laminins α4 and α5 in mediating these effects indicated a stromal response mechanism in immunosuppression driven laminin α4 and laminin α5 responses [14]. MMF and FTY both preserved tolerogenic LN architecture during allostimulation through the dual regulation of Tregs and stromal organization, while they were distinctively dependent on laminin α4 or laminin α5. Understanding these anatomically distinct and mechanistically diverse effects could lead to more precise immunosuppressive strategies that better maintain tolerogenic niches. Specifically, the precise effects of different immunosuppressive drugs on the gene expression, function and phenotype of LNSCs is a major gap in our knowledge and requires further investigations.

The major limitations in this study are our focus on mouse models and relatively short duration of study. The convergent effects at day 30 might not fully represent human responses, and longer-term studies may better reflect clinical scenarios. Additionally, we examined single drugs rather than combinations commonly used in practice. Our findings suggest specific therapeutic strategies such as metabolic monitoring to predict drug responses, targeted interventions to preserve microbiome dysbiosis, and tissue-specific drug delivery to optimize local effects while minimizing systemic complications.

Methods and Materials

Study approval

All procedures involving mice were performed in accordance with the guidelines and regulations set by the Office of Animal Welfare Assurance of the University of Maryland School of Medicine under the approved IACUC protocol nos. 05150001, 0318002, 1220001, and AUP-00000397.

Reagents

USP grade immunosuppressants were used if available. All drugs were prepared in a manner approved by the University of Maryland School of Medicine IACUC: TAC (USP grade, MilliporeSigma, Burlington, MA) was reconstituted in DMSO (USP grade, MilliporeSigma) at 20 mg/ml for storage. At time of use, TAC/DMSO stock was diluted with absolute ethanol (USP grade, Decon Labs, King of Prussia, PA) to 1.5 mg/ml then further diluted 1:5 in sterile PBS and injected at 10 µl/gm s.c. (3 mg/kg/day)[25]. PRED (MilliporeSigma) was reconstituted in PBS at 50 mg/ml for storage and then diluted to 0.5 mg/ml in PBS and injected at 5mg/kg/d i.p.[59]. MMF (MilliporeSigma) was reconstituted at 30 mg/ml in DMSO for storage and then diluted in PBS to 1.5 mg/ml and at 30 mg/kg/d i.p.[60]. FTY (Fingolimod, MilliporeSigma) was reconstituted at 3 mg/ml in 1:1 PBS:Ethanol for storage and then diluted 1:10 in PBS and administered at 3 mg/kg/d p.o.[61].

Mice

8- to 14-week-old female C57BL/6 mice between were purchased from The Jackson Laboratory (Bar Harbor, ME, USA). Mice were maintained at the University of Maryland

School of Medicine Veterinary Resources animal facility. Only female mice were used to ensure a high degree of homogeneity within our study groups. All procedures involving mice were performed in accordance with the guidelines and regulations set by the Office of Animal Welfare Assurance of the University of Maryland School of Medicine. Mice received daily immunosuppression following the dosages in the table above. During arrival at the animal facility, all mice were cohoused and handled together to ensure all groups were exposed to each other but separated during immunosuppressant treatment. CO_2 narcosis was utilized for euthanasia on the day of harvest. We collected intralumenal stool samples for metagenomic and metabolomic analyses. Blood collection was carried out using cardiac puncture at the time of euthanasia We acknowledge the potential effects of first-pass hepatic metabolism on general circulation, however, over extended periods, systemic metabolites should normalize, unless there are acute changes in the intestine that we did not observe within the experimental timeframe. Portal blood provides a more direct measure of metabolites absorbed from the intestine before they undergo hepatic metabolism. However, in mice, portal blood can only be reliably obtained at the time of euthanasia, and the obtainable volumes are exceedingly low, making its routine collection challenging. We collected mLN, pLN, and portions of the small intestine between the duodenum and jejunum, for immunohistochemistry. The mLN and pLN samples were harvested for flow cytometry analyses. Mouse experiments were performed according to ARRIVE guidelines (https://arriveguidelines.org).

Stool specimen collection, DNA extraction, and metagenomic sequencing

Mice jejunum and colon tissues were dissected according to their gastrointestinal anatomical features. From the dissected tissues, intraluminal stool contents were collected and stored immediately in DNA/RNA Shields (Zymo Research, Irvine, CA, USA) at -80°C. This stabilizes and protects the integrity of nucleic acids and minimizes the need for immediate processing or freezing of specimens. DNA extraction was described previously [62, 63]. In brief, the Quick-DNA Fecal/Soil Microbe kit (Zymo Research, Irvine, CA, USA) was used to extract 0.15-0.25 grams of fecal samples. To ensure that no exogenous DNA contaminated the samples, we includednegative extraction. Construction of metagenomic sequencing libraries was performed using the Nextera XT Flex Kit (Illumina), according to the manufacturer's recommendations. Then, libraries were pooled together in equimolar proportions before they were sequenced on a single Illumina NovaSeq 6000 S2 flow cell at Maryland Genomics at the University of Maryland School of Medicine.

Gut microbiome analyses

We removed metagenomic sequence reads using BMTagger v3.101 [64] mapping to Genome Reference Consortium Mouse Build 39 of strain C57BL/6J (GRCm39) [65]. When one or both of the read pairs matched the genome reference, sequence read pairs were removed. Trimming and quality assessment of the Illumina adapter was performed using default parameters in fastp (v.0.21.0) [66]. We established taxonomic composition of the microbiomes using Kraken2 (v.2020.12) [67] and Braken (v. 2.5.0) [68] and the comprehensive mouse gut metagenome catalog (CMGM) [34] to calculate the metagenomic taxonomic composition. Barplots and diversity indices were generated

using Phyloseq R package (v1.38.0) [69]. We employed the Chao1 diversity index, an abundance-based indicator of species richness (total number of species in a sample) that is sensitive to low abundance taxonomic groups (singletons and doubletons) [70] because the mice gut microbiome datasets contain a broad spectrum of taxa without any dominant high-abundance species. This choice ensures accurate representation and understanding of the microbial community diversity in our samples. To identify fecal phylotypes that could explain the differences, we utilized linear discriminant analysis (LDA) effect size (LEfSe) analysis [71]. For the non-paramentric factorial Kruskal Wallis (KW) sum-rank test, the α value was set at 0.05 and the threshold for the logarithmic LDA model [72] score for discriminative features was set at 2.0. In the multiclass analysis, an all-against-all BLAST search was performed. The limma voom function [73] in R package microbiomeMarker v1.3.3 [74] was used to calculate microbial biomarkers. Phylogram representing the taxonomic hierarchical structure of the identified phylotype biomarkers via pairwise comparisons between groups, graph generated using R package yingtools2 [75]. To ensure comprehensive coverage in functional annotation, the metagenomic dataset was mapped to the protein database UniRef90 [76]. To efficiently and accurately determine the presence, absence, and abundance of metabolic pathways in a microbial community, the dataset was then summarized using HUMAnN3 (Human Microbiome Project Unified Metabolic Analysis Network) (v3.0.0.alpha.3) [35]. Canonical Correspondence Analysis (CCA) utilizing the vegan package [77, 78] based on the Bray-Curtis distance was used for ordination analysis. Based on their eigenvalues, CA1 and CA2 were selected as the major components. To evaluate microbiome profile differences across groups and time points, the line plot was

generated using the average pairwise Bray-Curtis distances between all group pairs at each time point.

Metabolite extraction and metabolome analyses

Capillary electrophoresis-mass spectrometry (CE/MS) was used for measuring metabolome of intraluminal stool (luminal/local) to obtain a comprehensive quantitative survey of metabolites (Human Metabolome Technologies, Boston, MA, USA) for immunosuppressants TAC, PRED, MMF, and a no-treatment control group processed concurrently. For FTY720, stool pellets were collected at the same time points for metabolomic analysis due to technical limitations in obtaining sufficient sample volumes for comprehensive profiling. The no-treatment control for FTY720 also used stool pellets and processed concurrently. All subsequent analyses were performed using the respective no-treatment control groups and the same specimen types, processed concurrently with their corresponding experimental groups, to ensure valid comparisons. ~10-30 mg of stool was weighed at the time of collection using a company-provided vial and stored at -80°C until shipped to vendor on dry ice. Strict QC includes blanks and internal standards evenly spaced among samples and in every batch.

To reduce the influence of measurement noise, rigorous data pretreatment was performed according to validated procedures [79]. Log base 10 transformation was applied to individual values themselves, and data scaling adjusted each variable/feature by a scaling factor computed based on the range of each variable as the dispersion of the variable. Known metabolic databases or the *a priori* knowledge-based approach were used to exhaustively annotate metabolites, achieved using PubChem [80], KEGG

(vers Dec 2023) [81], HMDB [82], and MetaboAnalyst 5.0 [83, 84] annotation frameworks that leverage cataloged chemical compounds, known metabolic characterization, and functional hierarchy (i.e., reaction, modules, pathways). Partial least squares discriminant analysis (PLS-DA) implemented using mixOmics (vers. 6.18.1) was used [85]. To show significantly increased metabolites after 7-day tacrolimus treatment, the volcano plot combines results from fold change (FC) analysis. A metabolite is shown when the FC is >2 and the p-value is <0.05 based on 2-sample t-tests. In the FC analysis, original metabolite measurements without normalization were utilized. For the metabolites annotated in a specific functional pathway, metabolite set enrichment analysis (MSEA) was performed [86].

<u>RNA isolation, transcriptome sequencing and analyses of the intestinal tissues</u>

The colon tissues of the mice were dissected according to their anatomic features and stored immediately in RNAlater solution (QIAGEN) in RNAse-free 1.7-ml tubes (Denville Scientific, Holliston, MA) at -80°C to stabilize and protect the integrity of RNA. For each sample, total RNA was extracted from ~1 cm of ileum. Prior to the extraction, 500 µl of ice-cold RNase free PBS was added to the sample. To remove the RNAlater, the mixture was centrifuged at 8,000x*g* for 10 min and the resulting pellet resuspended in 500 µl ice-cold RNase-free PBS with 10 µl of β-mercaptoethanol. A tissue suspension was obtained by bead beating procedure using the FastPrep lysing matrix B protocol (MP Biomedicals, Solon, OH) to homogenized tissues. RNA was extracted from the resulting suspension using TRIzol Reagent (Invitrogen, Carlsbad, CA) following the manufacturer's recommendations and followed by protein cleanup using Phasemaker

tubes (Invitrogen) and precipitation of total nucleic acids using isopropanol. RNA was resuspended in DEPC-treated DNAase/RNAase-free water. Residual DNA was purged from total RNA extract by treating once with TURBO DNase (Ambion, Austin, TX, Cat. No. AM1907) according to the manufacturer's protocol. DNA removal was confirmed via PCR assay using 16S rRNA primer 27□F (5′-AGAGTTTGATCCTGGCTCAG-3′) and 534□R (5′-CATTACCGCGGCTGCTGG-3′). The quality of extracted RNA was verified using the Agilent 2100 Expert Bioanalyzer using the RNA 1000 Nano kit (Agilent Technologies, Santa Clara, CA). Ribosomal RNA depletion and library construction were performed using the RiboZero Plus kit and TruSeq stranded mRNA library preparation kit (Illumina) according to the manufacturer's recommendations. Libraries were then pooled together in equimolar proportions and sequenced on a single Illumina NovaSeq 6000 S2 flow cell at the Genomic Resource Center (Institute for Genome Sciences, University of Maryland School of Medicine) using the 150 bp paired-end protocol. An average of 87- 130 million reads were obtained for each sample. The quality of Fastq files was evaluated by using FastQC [87]. Reads were aligned to the mouse genome (Mus_musculus.GRCm39) using HiSat (version HISAT2-2.0.4) [88] and the number of reads that aligned to the coding regions was determined using HTSeq [89]. Significant differential expression was assessed using DEseq2 [90] with an FDR value ≤ 0.05 and FC>2. The over-representative analysis was done by importing Differentially Expressed Genes (DEGs) against GO ontologies using the enrichGO function of clusterProfile Bioconductor package [91]. Only the ontology terms with q value <0.05 were used for plotting. UpSet plots were generated using UpSetR (vers.

1.4.0) to analyze overlapping DEGs between days 7 and 30 and across different treatments.

Flow cytometry

To produce single-cell suspensions, LNs were disaggregated and passed through 70-µm nylon mesh screens (Thermo Fisher Scientific, Waltham, MA). Antibodies against surface molecules were incubated with cell suspensions for 30 min at 4°C (**Supplemental Table 4**) then washed with FACS buffer [PBS with 0.5% w/v bovine serum albumin] twice. Cells were then permeabilized, according to manufacturer's protocol, with Foxp3/Transcription Factor Staining Buffer Set (eBioscience, San Diego, CA), washed with FACS buffer, and subsequently stained with antibodies for intracellular molecules at 4°C. Samples were analyzed with an LSR Fortessa Cell Analyzer (BD Biosciences), and data were analyzed using FlowJo software version 10.6 (BD Biosciences).

Immunohistochemistry

We excised mLN, pLN and segments of the intestine then immediately submerged in OCT compound (Sakura Finetek, Torrance, CA, USA). Cryosections (6-7 µm for LNs, 10 µm for intestine) were cut in duplicate or triplicate depending on size of block using a Microm HM 550 cryostat (ThermoFisher Scientific). Slides were then fixed in cold 1:1 acetone:methanol for 5 min, air dried for 15 min, and stored at -80°C until use. At time of staining, slides were thawed for 15 minutes at room temperature then. sections were rehydrated in PBS and blocked with10% secondary antibody host serum PBST (PBS + 0.03% Triton-X-100 + 0.5% BSA). The slides were then stained for 1 hour with primary

antibodies at room temperature (diluted 1:50-1:200 in PBST) for 1 hour incubated with secondary antibodies (diluted 1:100-1:400 in PBST) for 1 hour. After staining, slides were fixed with 4% paraformaldehyde in PBS for 5 min, quenched with 1% glycerol in PBS for 5 min, and mounted with Prolong Gold Antifade Mountant with or without DAPI (Thermo Fisher Scientific). Images were acquired using a Nikon Accu-Scope EXC-500 (Nikon, Tokyo, Japan) and analyzed using Volocity software (PerkinElmer, Waltham, MA). The antibodies used are listed in **Supplemental Table 4**. More than 3 mice/group, 1-2 mLN or pLN or 3 pieces of intestine, 2-3 sections/tissue sample, and 7-30 fields/tissue sample were analyzed. We calculated mean fluorescence intensity (MFI) within demarcated high endothelial venules (HEV) and cortical ridge (CR) regions of the mLN and pLN as well as of intestinal images. Qualitative heat maps were generated (GraphPad prism) to express changes in IHC marker expression level relative to control using -1 to represent “decreased” (blue in the heatmap), 0 to represent “unchanged” (white in the heatmap), and 1 to represent “increased” (red in the heatmap). GraphPad Prism 10.3.1 was used for analysis (San Diego, CA, USA) with statistical significance defined as $P < 0.05$. Tukey’s multiple comparison tests of one-way ANOVA were used for comparisons of fluorescent.

Declarations

Ethics Approval and Consent to Participate

All experimental procedures involving mice were approved by and performed in accordance with the guidelines and regulations of the Institutional Animal Care and Use Committee (IACUC) of the University of Maryland School of Medicine under the approved protocol numbers 05150001, 0318002, 1220001, and AUP-0000397.

Consent for Publication

Not applicable.

Availability of data and materials

The authors confirm that the data supporting the findings of this study are available within the article and indicated supplementary materials. The data that support the findings of this study are openly available; metagenome sequences were submitted to GenBank under BioProject PRJNA809764 (https://www.ncbi.nlm.nih.gov/bioproject/PRJNA809764) with the SRA study ID SRP361281. The SRA accession numbers for each sample and their biosample ID are included in **Supplemental Table 1**. The R codes, including each step and parameters, were deposited in github at https://github.com/igsbma/omics_paper23. Supplemental data for this article can be accessed online at https://figshare.com/account/home#/projects/173364

Competing interests

No potential financial and non-financial conflict of interest was reported by the authors.

Acknowledgements

This work was supported by the National Institute of Health (NIH) National Heart, Lung and Blood Institute award R01HL148672 (JSB/BM), NIH National Institute of Allergy and Infectious Diseases U01AI170050 (BM/JSB/VM) and training grant T32AI95190-10 (SJG).

Authors' contributions

B. M., and J. S. B. designed the experiments. L. W., A. K., S. J. G., V. S., W. P., R. L., J. I., M. W., and L. L. conducted and analyzed the mice experiments. H. W. L. performed nucleic acid extraction and sequencing library preparation. B. M. and Y. S. performed the bioinformatics analyses. B. M., L. W., A. K., S. J. G., M. F., and J. S. B. wrote the manuscript. B. M. and J. S. B. are co-corresponding authors for this manuscript.

References

1. Lodhi SA, Lamb KE, Meier-Kriesche HU: **Solid Organ Allograft Survival Improvement in the United States: The Long-Term Does Not Mirror the Dramatic Short-Term Success**. *American Journal of Transplantation* 2011, **11**(6):1226-1235.
2. Dai H, Zheng Y, Thomson AW, Rogers NM: **Transplant Tolerance Induction: Insights From the Liver**. *Frontiers in Immunology* 2020, **11**.
3. Fishman JA: **Infection in Organ Transplantation**. *Am J Transplant* 2017, **17**(4):856-879.
4. Gallagher MP, Kelly PJ, Jardine M, Perkovic V, Cass A, Craig JC, Eris J, Webster AC: **Long-term cancer risk of immunosuppressive regimens after kidney transplantation**. *J Am Soc Nephrol* 2010, **21**(5):852-858.
5. Schmitz V, Klawitter J, Bendrick-Peart J, Schoening W, Puhl G, Haschke M, Klawitter J, Consoer J, Rivard CJ, Chan L *et al*: **Metabolic profiles in urine reflect nephrotoxicity of sirolimus and cyclosporine following rat kidney transplantation**. *Nephron Exp Nephrol* 2009, **111**(4):e80-91.
6. Gioco R, Corona D, Ekser B, Puzzo L, Inserra G, Pinto F, Schipa C, Privitera F, Veroux P, Veroux M: **Gastrointestinal complications after kidney transplantation**. *World J Gastroenterol* 2020, **26**(38):5797-5811.
7. Wijdicks EF: **Neurotoxicity of immunosuppressive drugs**. *Liver Transpl* 2001, **7**(11):937-942.
8. Bhat M, Usmani SE, Azhie A, Woo M: **Metabolic Consequences of Solid Organ Transplantation**. *Endocr Rev* 2021, **42**(2):171-197.
9. Nayak SP, Bagchi B, Roy S: **Effects of immunosuppressants on T-cell dynamics: Understanding from a generic coarse-grained immune network model**. *J Biosci* 2022, **47**(4).
10. Xie H, Zhu H, Zhou K, Wan J, Zhang L, Yang Z, Zhou L, Chen X, Xu X, Zheng S *et al*: **Target-oriented delivery of self-assembled immunosuppressant cocktails prolongs allogeneic orthotopic liver transplant survival**. *J Control Release* 2020, **328**:237-250.
11. Saxena V, Li L, Paluskievicz C, Kasinath V, Bean A, Abdi R, Jewell CM, Bromberg JS: **Role of lymph node stroma and microenvironment in T cell tolerance**. *Immunol Rev* 2019, **292**(1):9-23.
12. Li L, Wu J, Abdi R, Jewell CM, Bromberg JS: **Lymph node fibroblastic reticular cells steer immune responses**. *Trends Immunol* 2021, **42**(8):723-734.
13. Mueller SN, Hosiawa-Meagher KA, Konieczny BT, Sullivan BM, Bachmann MF, Locksley RM, Ahmed R, Matloubian M: **Regulation of homeostatic chemokine expression and cell trafficking during immune responses**. *Science* 2007, **317**(5838):670-674.
14. Li L, Shirkey MW, Zhang T, Xiong Y, Piao W, Saxena V, Paluskievicz C, Lee Y, Toney N, Cerel BM *et al*: **The lymph node stromal laminin alpha5 shapes alloimmunity**. *J Clin Invest* 2020, **130**(5):2602-2619.
15. Simon T, Li L, Wagner C, Zhang T, Saxena V, Brinkman CC, Tostanoski LH, Ostrand-Rosenberg S, Jewell C, Shea-Donohue T *et al*: **Differential Regulation of T-cell Immunity and Tolerance by Stromal Laminin Expressed in the Lymph Node**. *Transplantation* 2019, **103**(10):2075-2089.

782 16. Maarouf OH, Uehara M, Kasinath V, Solhjou Z, Banouni N, Bahmani B, Jiang L, Yilmam
783 OA, Guleria I, Lovitch SB *et al*: **Repetitive ischemic injuries to the kidneys result in**
784 **lymph node fibrosis and impaired healing**. *JCI Insight* 2018, **3**(13).
785 17. Mongodin EF, Saxena V, Iyyathurai J, Lakhan R, Ma B, Silverman E, Lee ZL, Bromberg JS:
786 **Chronic rejection as a persisting phantom menace in organ transplantation: a new**
787 **hope in the microbiota?** *Curr Opin Organ Transplant* 2021, **26**(6):567-581.
788 18. Lei YM, Chen L, Wang Y, Stefka AT, Molinero LL, Theriault B, Aquino-Michaels K, Sivan AS,
789 Nagler CR, Gajewski TF *et al*: **The composition of the microbiota modulates allograft**
790 **rejection**. *J Clin Invest* 2016, **126**(7):2736-2744.
791 19. Hossain MS, Jaye DL, Pollack BP, Farris AB, Tselanyane ML, David E, Roback JD, Gewirtz
792 AT, Waller EK: **Flagellin, a TLR5 agonist, reduces graft-versus-host disease in allogeneic**
793 **hematopoietic stem cell transplantation recipients while enhancing antiviral immunity**.
794 *J Immunol* 2011, **187**(10):5130-5140.
795 20. Jenq RR, Ubeda C, Taur Y, Menezes CC, Khanin R, Dudakov JA, Liu C, West ML, Singer NV,
796 Equinda MJ *et al*: **Regulation of intestinal inflammation by microbiota following**
797 **allogeneic bone marrow transplantation**. *J Exp Med* 2012, **209**(5):903-911.
798 21. Oh PL, Martinez I, Sun Y, Walter J, Peterson DA, Mercer DF: **Characterization of the ileal**
799 **microbiota in rejecting and nonrejecting recipients of small bowel transplants**. *Am J*
800 *Transplant* 2012, **12**(3):753-762.
801 22. Willner DL, Hugenholtz P, Yerkovich ST, Tan ME, Daly JN, Lachner N, Hopkins PM,
802 Chambers DC: **Reestablishment of recipient-associated microbiota in the lung allograft**
803 **is linked to reduced risk of bronchiolitis obliterans syndrome**. *Am J Respir Crit Care*
804 *Med* 2013, **187**(6):640-647.
805 23. Koren O, Goodrich JK, Cullender TC, Spor A, Laitinen K, Backhed HK, Gonzalez A, Werner
806 JJ, Angenent LT, Knight R *et al*: **Host remodeling of the gut microbiome and metabolic**
807 **changes during pregnancy**. *Cell* 2012, **150**(3):470-480.
808 24. Rooks MG, Veiga P, Wardwell-Scott LH, Tickle T, Segata N, Michaud M, Gallini CA, Beal C,
809 van Hylckama-Vlieg JE, Ballal SA *et al*: **Gut microbiome composition and function in**
810 **experimental colitis during active disease and treatment-induced remission**. *The ISME*
811 *journal* 2014, **8**(7):1403-1417.
812 25. Bromberg JS, Hittle L, Xiong Y, Saxena V, Smyth EM, Li L, Zhang T, Wagner C, Fricke WF,
813 Simon T *et al*: **Gut microbiota-dependent modulation of innate immunity and lymph**
814 **node remodeling affects cardiac allograft outcomes**. *JCI Insight* 2018, **3**(19).
815 26. Ma B, Gavzy SJ, France M, Song Y, Lwin HW, Kensiski A, Saxena V, Piao W, Lakhan R,
816 Iyyathurai J *et al*: **Rapid intestinal and systemic metabolic reprogramming in an**
817 **immunosuppressed environment**. *BMC Microbiol* 2023, **23**(1):394.
818 27. Gao Y, Tian T: **mTOR Signaling Pathway and Gut Microbiota in Various Disorders:**
819 **Mechanisms and Potential Drugs in Pharmacotherapy**. *Int J Mol Sci* 2023, **24**(14).
820 28. Liu Y, Yang F, Zou S, Qu L: **Rapamycin: A Bacteria-Derived Immunosuppressant That**
821 **Has Anti-atherosclerotic Effects and Its Clinical Application**. *Front Pharmacol* 2018,
822 **9**:1520.
823 29. Nayak RR, Alexander M, Deshpande I, Stapleton-Gray K, Rimal B, Patterson AD, Ubeda C,
824 Scher JU, Turnbaugh PJ: **Methotrexate impacts conserved pathways in diverse human**

825 **gut bacteria leading to decreased host immune activation**. *Cell Host Microbe* 2021,
826 **29**(3):362-377 e311.
827 30. Khan N, Binder L, Pantakani DVK, Asif AR: **MPA Modulates Tight Junctions' Permeability**
828 **via Midkine/PI3K Pathway in Caco-2 Cells: A Possible Mechanism of Leak-Flux Diarrhea**
829 **in Organ Transplanted Patients**. *Frontiers in physiology* 2017, **8**:438.
830 31. Wilson ID, Nicholson JK: **Gut microbiome interactions with drug metabolism, efficacy,**
831 **and toxicity**. *Transl Res* 2017, **179**:204-222.
832 32. Haiser HJ, Gootenberg DB, Chatman K, Sirasani G, Balskus EP, Turnbaugh PJ: **Predicting**
833 **and manipulating cardiac drug inactivation by the human gut bacterium Eggerthella**
834 **lenta**. *Science* 2013, **341**(6143):295-298.
835 33. Taylor MR, Flannigan KL, Rahim H, Mohamud A, Lewis IA, Hirota SA, Greenway SC:
836 **Vancomycin relieves mycophenolate mofetil-induced gastrointestinal toxicity by**
837 **eliminating gut bacterial beta-glucuronidase activity**. *Sci Adv* 2019, **5**(8):eaax2358.
838 34. Kieser S, Zdobnov EM, Trajkovski M: **Comprehensive mouse gut metagenome catalog**
839 **reveals major difference to the human counterpart**. *bioRxiv*
840 2021:2021.2003.2018.435958.
841 35. Franzosa EA, McIver LJ, Rahnavard G, Thompson LR, Schirmer M, Weingart G, Lipson KS,
842 Knight R, Caporaso JG, Segata N *et al*: **Species-level functional profiling of**
843 **metagenomes and metatranscriptomes**. *Nat Methods* 2018, **15**(11):962-968.
844 36. Yang X, Wang Z, Niu J, Zhai R, Xue X, Wu G, Fang Y, Meng G, Yuan H, Zhao L *et al*:
845 **Pathobionts from chemically disrupted gut microbiota induce insulin-dependent**
846 **diabetes in mice**. *Microbiome* 2023, **11**(1):62.
847 37. Warren KJ, Iwami D, Harris DG, Bromberg JS, Burrell BE: **Laminins affect T cell trafficking**
848 **and allograft fate**. *J Clin Invest* 2014, **124**(5):2204-2218.
849 38. Kato T, Chan MC, Gao SZ, Schroeder JS, Yokota M, Murohara T, Iwase M, Noda A, Hunt
850 SA, Valantine HA: **Glucose intolerance, as reflected by hemoglobin A1c level, is**
851 **associated with the incidence and severity of transplant coronary artery disease**. *J Am*
852 *Coll Cardiol* 2004, **43**(6):1034-1041.
853 39. Valantine H, Rickenbacker P, Kemna M, Hunt S, Chen YD, Reaven G, Stinson EB:
854 **Metabolic abnormalities characteristic of dysmetabolic syndrome predict the**
855 **development of transplant coronary artery disease: a prospective study**. *Circulation*
856 2001, **103**(17):2144-2152.
857 40. Biadi O, Potena L, Fearon WF, Luikart HI, Yeung A, Ferrara R, Hunt SA, Mocarski ES,
858 Valantine HA: **Interplay between systemic inflammation and markers of insulin**
859 **resistance in cardiovascular prognosis after heart transplantation**. *J Heart Lung*
860 *Transplant* 2007, **26**(4):324-330.
861 41. Scott LJ, McKeage K, Keam SJ, Plosker GL: **Tacrolimus: a further update of its use in the**
862 **management of organ transplantation**. *Drugs* 2003, **63**(12):1247-1297.
863 42. Rhen T, Cidlowski JA: **Antiinflammatory action of glucocorticoids--new mechanisms for**
864 **old drugs**. *N Engl J Med* 2005, **353**(16):1711-1723.
865 43. van Raalte DH, Ouwens DM, Diamant M: **Novel insights into glucocorticoid-mediated**
866 **diabetogenic effects: towards expansion of therapeutic options?** *Eur J Clin Invest* 2009,
867 **39**(2):81-93.

868 44. Compston J: **Glucocorticoid-induced osteoporosis: an update**. *Endocrine* 2018, **61**(1):7-
869 16.
870 45. Eastell R, Reid DM, Compston J, Cooper C, Fogelman I, Francis RM, Hosking DJ, Purdie
871 DW, Ralston SH, Reeve J *et al*: **A UK Consensus Group on management of**
872 **glucocorticoid-induced osteoporosis: an update**. *J Intern Med* 1998, **244**(4):271-292.
873 46. Shipkova M, Armstrong VW, Oellerich M, Wieland E: **Acyl glucuronide drug metabolites:**
874 **toxicological and analytical implications**. *Ther Drug Monit* 2003, **25**(1):1-16.
875 47. Oellerich M, Shipkova M, Schutz E, Wieland E, Weber L, Tonshoff B, Armstrong VW:
876 **Pharmacokinetic and metabolic investigations of mycophenolic acid in pediatric**
877 **patients after renal transplantation: implications for therapeutic drug monitoring.**
878 **German Study Group on Mycophenolate Mofetil Therapy in Pediatric Renal Transplant**
879 **Recipients**. *Ther Drug Monit* 2000, **22**(1):20-26.
880 48. Helderman JH, Goral S: **Gastrointestinal complications of transplant**
881 **immunosuppression**. *J Am Soc Nephrol* 2002, **13**(1):277-287.
882 49. Enoru JO, Yang B, Krishnamachari S, Villanueva E, DeMaio W, Watanyar A, Chinnasamy R,
883 Arterburn JB, Perez RG: **Preclinical Metabolism, Pharmacokinetics and In Vivo Analysis**
884 **of New Blood-Brain-Barrier Penetrant Fingolimod Analogues: FTY720-C2 and FTY720-**
885 **Mitoxy**. *PLoS One* 2016, **11**(9):e0162162.
886 50. Bhat M, Pasini E, Copeland J, Angeli M, Husain S, Kumar D, Renner E, Teterina A, Allard J,
887 Guttman DS *et al*: **Impact of Immunosuppression on the Metagenomic Composition of**
888 **the Intestinal Microbiome: a Systems Biology Approach to Post-Transplant Diabetes**.
889 *Sci Rep* 2017, **7**(1):10277.
890 51. Toral M, Romero M, Rodriguez-Nogales A, Jimenez R, Robles-Vera I, Algieri F, Chueca-
891 Porcuna N, Sanchez M, de la Visitacion N, Olivares M *et al*: **Lactobacillus fermentum**
892 **Improves Tacrolimus-Induced Hypertension by Restoring Vascular Redox State and**
893 **Improving eNOS Coupling**. *Mol Nutr Food Res* 2018, **62**(14):e1800033.
894 52. Robles-Vera I, Toral M, de la Visitacion N, Sanchez M, Gomez-Guzman M, Romero M,
895 Yang T, Izquierdo-Garcia JL, Jimenez R, Ruiz-Cabello J *et al*: **Probiotics Prevent Dysbiosis**
896 **and the Rise in Blood Pressure in Genetic Hypertension: Role of Short-Chain Fatty**
897 **Acids**. *Mol Nutr Food Res* 2020, **64**(6):e1900616.
898 53. Wang S, Lu J, You Q, Huang H, Chen Y, Liu K: **The mTOR/AP-1/VEGF signaling pathway**
899 **regulates vascular endothelial cell growth**. *Oncotarget* 2016, **7**(33):53269-53276.
900 54. Wang Y, Li Q, Zhang Z, Peng K, Zhang DM, Yang Q, Passerini AG, Simon SI, Sun C: **mTOR**
901 **contributes to endothelium-dependent vasorelaxation by promoting eNOS expression**
902 **and preventing eNOS uncoupling**. *Commun Biol* 2022, **5**(1):726.
903 55. Rodrigues-Diez R, Gonzalez-Guerrero C, Ocana-Salceda C, Rodrigues-Diez RR, Egido J,
904 Ortiz A, Ruiz-Ortega M, Ramos AM: **Calcineurin inhibitors cyclosporine A and**
905 **tacrolimus induce vascular inflammation and endothelial activation through TLR4**
906 **signaling**. *Sci Rep* 2016, **6**:27915.
907 56. Honda K, Littman DR: **The microbiota in adaptive immune homeostasis and disease**.
908 *Nature* 2016, **535**(7610):75-84.
909 57. Gabarre P, Loens C, Tamzali Y, Barrou B, Jaisser F, Tourret J: **Immunosuppressive**
910 **therapy after solid organ transplantation and the gut microbiota: Bidirectional**
911 **interactions with clinical consequences**. *Am J Transplant* 2022, **22**(4):1014-1030.

912 58. Salvadori M, Rosso G: **Update on the reciprocal interference between**
913 **immunosuppressive therapy and gut microbiota after kidney transplantation**. *World J*
914 *Transplant* 2024, **14**(1):90194.
915 59. Chin HJ, Chae DW, Kim YC, An WS, Ihm C, Jin DC, Kim SG, Kim YL, Kim YS, Kim YG *et al*:
916 **Comparison of the Efficacy and Safety of Tacrolimus and Low-Dose Corticosteroid with**
917 **High-Dose Corticosteroid for Minimal Change Nephrotic Syndrome in Adults**. *J Am Soc*
918 *Nephrol* 2021, **32**(1):199-210.
919 60. Richez C, Richards RJ, Duffau P, Weitzner Z, Andry CD, Rifkin IR, Aprahamian T: **The**
920 **effect of mycophenolate mofetil on disease development in the gld.apoE (-/-) mouse**
921 **model of accelerated atherosclerosis and systemic lupus erythematosus**. *PLoS One*
922 2013, **8**(4):e61042.
923 61. Honig SM, Fu S, Mao X, Yopp A, Gunn MD, Randolph GJ, Bromberg JS: **FTY720 stimulates**
924 **multidrug transporter– and cysteinyl leukotriene–dependent T cell chemotaxis to**
925 **lymph nodes**. *Journal of Clinical Investigation* 2003, **111**(5):627-637.
926 62. Bromberg JS, Hittle LE, Xiong Y, Saxena V, Smyth EM, Li L, Zhang T, Wagner C, Fricke WF,
927 Simon T *et al*: **Gut microbiota–dependent modulation of innate immunity and lymph**
928 **node remodeling affects cardiac allograft outcomes**. *JCI Insight* 2018, **3**(19).
929 63. Ma B, Gavzy SJ, Saxena V, Song Y, Piao W, Lwin HW, Lakhan R, Iyyathurai J, Li L, France
930 M *et al*: **Strain-specific alterations in gut microbiome and host immune responses**
931 **elicited by tolerogenic Bifidobacterium pseudolongum**. *Sci Rep* 2023, **13**(1):1023.
932 64. Rotmistrovsky K, Agarwala R: **BMTagger: Best Match Tagger for removing human reads**
933 **from metagenomics datasets**. In.: NCBI/NLM, National Institutes of Health; 2011.
934 65. Church DM, Schneider VA, Graves T, Auger K, Cunningham F, Bouk N, Chen HC, Agarwala
935 R, McLaren WM, Ritchie GR *et al*: **Modernizing reference genome assemblies**. *PLoS Biol*
936 2011, **9**(7):e1001091.
937 66. Chen S, Zhou Y, Chen Y, Gu J: **fastp: an ultra-fast all-in-one FASTQ preprocessor**.
938 *Bioinformatics* 2018, **34**(17):i884-i890.
939 67. Wood DE, Lu J, Langmead B: **Improved metagenomic analysis with Kraken 2**. *Genome*
940 *Biol* 2019, **20**(1):257.
941 68. Lu J, Breitwieser FP, Thielen P, SL S: **Bracken: estimating species abundance in**
942 **metagenomics data**. *PeerJ Computer Science* 2017, **3**:e104.
943 69. McMurdie PJ, Holmes S: **phyloseq: an R package for reproducible interactive analysis**
944 **and graphics of microbiome census data**. *PLoS One* 2013, **8**(4):e61217.
945 70. Chao A: **Estimating the population size for capture-recapture data with unequal**
946 **catchability**. *Biometrics* 1987, **43**(4):783-791.
947 71. Segata N, Izard J, Waldron L, Gevers D, Miropolsky L, Garrett WS, Huttenhower C:
948 **Metagenomic biomarker discovery and explanation**. *Genome Biol* 2011, **12**(6):R60.
949 72. Fisher RA: **The use of multiple measurements in taxonomic problems.** *Ann Eugenics*
950 1936, **7**(179-188).
951 73. Law CW, Chen Y, Shi W, Smyth GK: **voom: Precision weights unlock linear model**
952 **analysis tools for RNA-seq read counts**. *Genome Biol* 2014, **15**(2):R29.
953 74. Cao Y, Dong Q, Wang D, Zhang P, Liu Y, Niu C: **microbiomeMarker: an R/Bioconductor**
954 **package for microbiome marker identification and visualization**. *Bioinformatics* 2022,
955 **38**(16):4027-4029.

75. **yingtools2 package** [https://github.com/ying14/yingtools2]
76. Kanehisa M, Goto S, Sato Y, Furumichi M, Tanabe M: **KEGG for integration and interpretation of large-scale molecular data sets**. *Nucleic Acids Res* 2012, **40**(Database issue):D109-114.
77. Jari Oksanen FGB, Michael Friendly, Roeland Kindt, Pierre Legendre, Dan McGlinn, Peter R. Minchin, R. B. O'Hara, Gavin L. Simpson, Peter Solymos, M. Henry H. Stevens, Eduard Szoecs and Helene Wagner **vegan: Community Ecology Package. R package**. In., version 2.4-1. edn; 2016.
78. Dixon P: **VEGAN, a package of R functions for community ecology**. *Journal of Vegetation Science* 2003, **14**(6):927-930.
79. van den Berg RA, Hoefsloot HC, Westerhuis JA, Smilde AK, van der Werf MJ: **Centering, scaling, and transformations: improving the biological information content of metabolomics data**. *BMC Genomics* 2006, **7**:142.
80. Kim S, Chen J, Cheng T, Gindulyte A, He J, He S, Li Q, Shoemaker BA, Thiessen PA, Yu B *et al*: **PubChem in 2021: new data content and improved web interfaces**. *Nucleic Acids Res* 2021, **49**(D1):D1388-D1395.
81. Hattori M, Tanaka N, Kanehisa M, Goto S: **SIMCOMP/SUBCOMP: chemical structure search servers for network analyses**. *Nucleic Acids Res* 2010, **38**(Web Server issue):W652-656.
82. Wishart DS, Feunang YD, Marcu A, Guo AC, Liang K, Vazquez-Fresno R, Sajed T, Johnson D, Li C, Karu N *et al*: **HMDB 4.0: the human metabolome database for 2018**. *Nucleic Acids Res* 2018, **46**(D1):D608-D617.
83. Pang Z, Chong J, Zhou G, de Lima Morais DA, Chang L, Barrette M, Gauthier C, Jacques PE, Li S, Xia J: **MetaboAnalyst 5.0: narrowing the gap between raw spectra and functional insights**. *Nucleic Acids Res* 2021, **49**(W1):W388-W396.
84. Pang Z, Zhou G, Ewald J, Chang L, Hacariz O, Basu N, Xia J: **Using MetaboAnalyst 5.0 for LC-HRMS spectra processing, multi-omics integration and covariate adjustment of global metabolomics data**. *Nat Protoc* 2022, **17**(8):1735-1761.
85. Le Cao KA, Boitard S, Besse P: **Sparse PLS discriminant analysis: biologically relevant feature selection and graphical displays for multiclass problems**. *BMC Bioinformatics* 2011, **12**:253.
86. Xia J, Wishart DS: **MSEA: a web-based tool to identify biologically meaningful patterns in quantitative metabolomic data**. *Nucleic Acids Res* 2010, **38**(Web Server issue):W71-77.
87. **FastQC: A Quality Control Tool for High Throughput Sequence Data** [Available online at: http://www.bioinformatics.babraham.ac.uk/projects/fastqc/]
88. Kim D, Langmead B, Salzberg SL: **HISAT: a fast spliced aligner with low memory requirements**. *Nat Methods* 2015, **12**(4):357-360.
89. Anders S, Pyl PT, Huber W: **HTSeq--a Python framework to work with high-throughput sequencing data**. *Bioinformatics* 2015, **31**(2):166-169.
90. Anders S, Huber W: **Differential expression analysis for sequence count data**. *Genome Biol* 2010, **11**(10):R106.

998 91. G. Yu, L. Wang, Y. Han, He Q: **clusterProfiler: an R package for comparing biological**
999 **themes among gene clusters.** *OMICS: A Journal of Integrative Biology* 2012, **16**(5):284-
1000 287.
1001 92. Bromberg JS, Hittle L, Xiong Y, Saxena V, Smyth EM, Li L, Zhang T, Wagner C, Fricke WF,
1002 Simon T *et al*: **Gut microbiota–dependent modulation of innate immunity and lymph**
1003 **node remodeling affects cardiac allograft outcomes**. *JCI Insight* 2018, **3**(19).
1004 93. Beeton C, Richez C, Richards RJ, Duffau P, Weitzner Z, Andry CD, Rifkin IR, Aprahamian T:
1005 **The Effect of Mycophenolate Mofetil on Disease Development in the gld.apoE−/−**
1006 **Mouse Model of Accelerated Atherosclerosis and Systemic Lupus Erythematosus**. *PLoS*
1007 *ONE* 2013, **8**(4):e61042.
1008 94. Honig SM, Fu S, Mao X, Yopp A, Gunn MD, Randolph GJ, Bromberg JS: **FTY720 stimulates**
1009 **multidrug transporter- and cysteinyl leukotriene-dependent T cell chemotaxis to**
1010 **lymph nodes**. *Journal of Clinical Investigation* 2003, **111**(5):627-637.
1011

Tables

Table 1. Differential metabolite abundance in gut lumen after 7 days of immunosuppressant treatment *

	TAC	PRED	MMF	FTY720
↑	**31** • Amino acids & derivatives • Pyrimidine metabolism • Sugars and sugar phosphates	**4** • Amino acids & derivatives	**4** • Sugar phosphates • Adenosine	**14** • Purine metabolism • Arginine metabolism
↓	**28** • Polyamines & derivatives • SCFAs, TMA	**95** • Amino acids & derivatives • SCFAs, TMA • Pyrimidine metabolism • Polyamines & derivatives	**37** • Glyoxylate and Dicarboxylate • Branched-chain amino acids & derivatives • Purine metabolism • Neurotransmitters	**22** • Pyrimidine metabolism • SCFAs
subtotal	**59**	**99**	**41**	**36**

* Gut luminal metabolites with significant changes (fold change >2, $p<0.05$) after 7 days of treatment with tacrolimus (TAC), prednisone (PRED), mycophenolate mofetil (MMF), or FTY720 compared to untreated controls. Numbers in bold indicate total metabolites significantly increased (↑) or decreased (↓) for each drug. Key metabolic pathways affected are listed for each drug. SCFAs: short-chain fatty acids; TMA: trimethylamine. Data derived from untargeted metabolomics analysis using capillary electrophoresis-mass spectrometry.

Table 2. Immunosuppression drugs and dosage.

Treatment Groups	Dose*(mg/kg/day)	Source (catalog #)	Route
Tacrolimus	3 mg/kg/day	Sigma Aldrich (Y0001926)	Subcutaneous [92]
Prednisolone	5 mg/kg/day	Sigma Aldrich (P6004)	Intraperitoneal [59]
Mycophenolate mofetil	30 mg/kg/day	Sigma Aldrich (SML0284)	Intraperitoneal [93]
FTY720	3 mg/kg/day	Sigma Aldrich **(**SML0700**)**	Oral [94]

Figure legends

Figure 1: Immunosuppressants dynamically influence gut microbiome. Mean pairwise distance comparison between conditions using gut microbiome **A)** taxonomic profiles and **B)** functional pathway profiles. Both taxonomic and functional pathways profiles are relative abundance of taxonomic groups. Distance calculated based on average Bray-Curtis distance per group. **C**) Principal Components Analysis of gut microbiome. Robust centered log ratio transformation applied on count compositional data, PCA calculated based on Bray-Curtis distance. **D)** Differentially abundant taxonomic groups. No treatment control group for comparison. Pairwise comparisons between the relative abundance of taxonomic groups and no treatment control. Fold changes in taxonomic group abundance expressed using base 2 logarithmic ratio.

Figure 2: Immunosuppressants distinctively influence gut metabolism. Volcano plots combine results from fold change (FC) analysis to show significantly increased metabolites after 7 days for **A**) TAC, **B**) PRED, **C**) MMF, or **D**) FTY720 treatment compared to no treatment control. A metabolite is shown if FC is >2 and p value is <0.05 based on 2-sample t-tests. Original metabolite measurement without normalization in FC analysis.

Figure 3: Immunosuppressants temporally shift intestinal immune responses. A) Bar plots showing the number of differentially expressed genes (DEGs) after 7 and 30 days of treatment compared to the control group. Yellow and blue bars indicate the number of upregulated genes, while red and green bars represent the number of

downregulated genes. **B**) Dot plot illustrating over-represented immune-related functional pathways of DEGs in small intestinal tissues across different treatments compared to the control group, analyzed at 7 and 30 days of treatment. Gene Ontology pathways used. Dot size represents the -log10(p-value), indicating the statistical significance of pathway enrichment.

Figure 4: Effects of TAC, PRED, MMF, and FTY720 on mLN cell content, cell distribution, and structure. Flow cytometry analysis of **A)** B220+ B cells and CD4+ T cells on day 30 after PRED treatment and **B)** Foxp3+ Tregs on day 30 after FTY treatment in mLNs. **C)** Heatmaps depict changes in expression with TAC, PRED, MMF, and FTY relative to control in mLN after 3, 7, and 30 days of treatment. IHC of **D)** CR and **E)** HEV Foxp3+ Tregs on days 3, 7, and 30 of mLN. IHC of **F)** CR and **G)** HEV la4: la5 on days 3, 7, and 30 of mLN. Barplot showing detailed plots at each timepoint are in **Supplemental Figure 6.** Heatmaps depict changes in expression with tacrolimus, prednisolone, MMF, and FTY720 relative to control in **H)** CR and **I)** around HEV in mLN. 3 mice/group. 2-3 LNs/mouse, 2-3 sections/LN, 7-30 fields/tissue. One-way ANOVA. * $p < 0.05$; ** $p < 0.01$, *** $p < 0.001$, **** $p < 0.0001$.

Figure 5: Effects of TAC, PRED, MMF, and FTY720 on pLN cell content, cell distribution, and structure. Flow cytometry analysis of **A)** CD4+ T cells on day 30 after MMF treatment, **B)** B220+ B cells and CD4+ T cells on day 7 and **C)** CD4+ T cells and Foxp3+ Tregs after FTY treatment in pLNs. **D)** Heatmaps depict changes in expression with TAC, PRED, MMF, and FTY relative to control in pLN after 3, 7, and 30

days of treatment. IHC of **E)** CR and **F)** HEV Foxp3+ Tregs on days 3, 7, and 30 of pLN. IHC of **G)** CR and **H)** la4: la5 on days 3, 7, and 30 of pLN. Barplot showing detailed plots at each timepoint are in **Supplemental Figure 7.** Heatmaps depict changes in expression with tacrolimus, prednisolone, MMF, and FTY720 relative to control in **I)** CR and **J)** around HEV in pLN. 3 mice/group. 2-3 LNs/mouse, 2-3 sections/LN, 7-30 fields/tissue. One-way ANOVA. * $p < 0.05$; ** $p < 0.01$, *** $p < 0.001$, **** $p < 0.0001$.

Figure 6. MMF and FTY720 induce a rapid anti-inflammatory response during allogeneic stimulation. IHC for Foxp3+ Tregs in the **A**) pLN and **C**) mLN. La4:La5 in **B**) pLN and **D**) mLN. Heatmap summarizes significant changes in expression comparing allogeneic stimulation plus MMF or FTY720 to allogeneic stimulation alone in **E**) pLN and **F**) mLN. 3 mice/group. 2-3 LNs/mouse, 2-3 sections/LN, 7-30 fields/tissue. One-way ANOVA: * $p < 0.05$, ** $p < 0.01$, *** $p < 0.001$, **** $p < 0.0001$.

Figure 7. MMF and FTY decrease the La4:La5 in FRC-Lama5-KO mLN. IHC showing **A, D**) laminin α4; **B, E**) laminin α5; and **C, F**) La4:La5 in mLN of WT, FRC-Lama4-KO mice (**A-C**) and FRC-Lama5-KO mice (**D-F**) on day 3. **G**) Heatmap summarizes significant changes relative to control. 3-5 mice/group. 2-3 LNs/mouse, 2-3 sections/LN, 7-30 fields/tissue. One-way ANOVA: * $p < 0.05$, ** $p < 0.01$, *** $p < 0.001$, **** $p < 0.0001$.

Figure 8. MMF increases the La4:La5 in FRC-Lama5-KO, and FTY decreases the La4:La5 in FRC-Lama4-KO pLN. IHC for **A, D**) laminin α4; **B, E**) laminin α5; and **C, F**)

La4:La5 in pLN WT, FRC-Lama4-KO mice (**A-C**) and FRC-Lama5-KO mice (**D-F**) on day 3. **G**) Heatmap summarizes significant changes relative to control. 3-5 mice/group. 2-3 LNs/mouse, 2-3 sections/LN, 7-30 fields/tissue. One-way ANOVA* $p < 0.05$, ** $p < 0.01$, *** $p < 0.001$, **** $p < 0.0001$.

Figure 1.

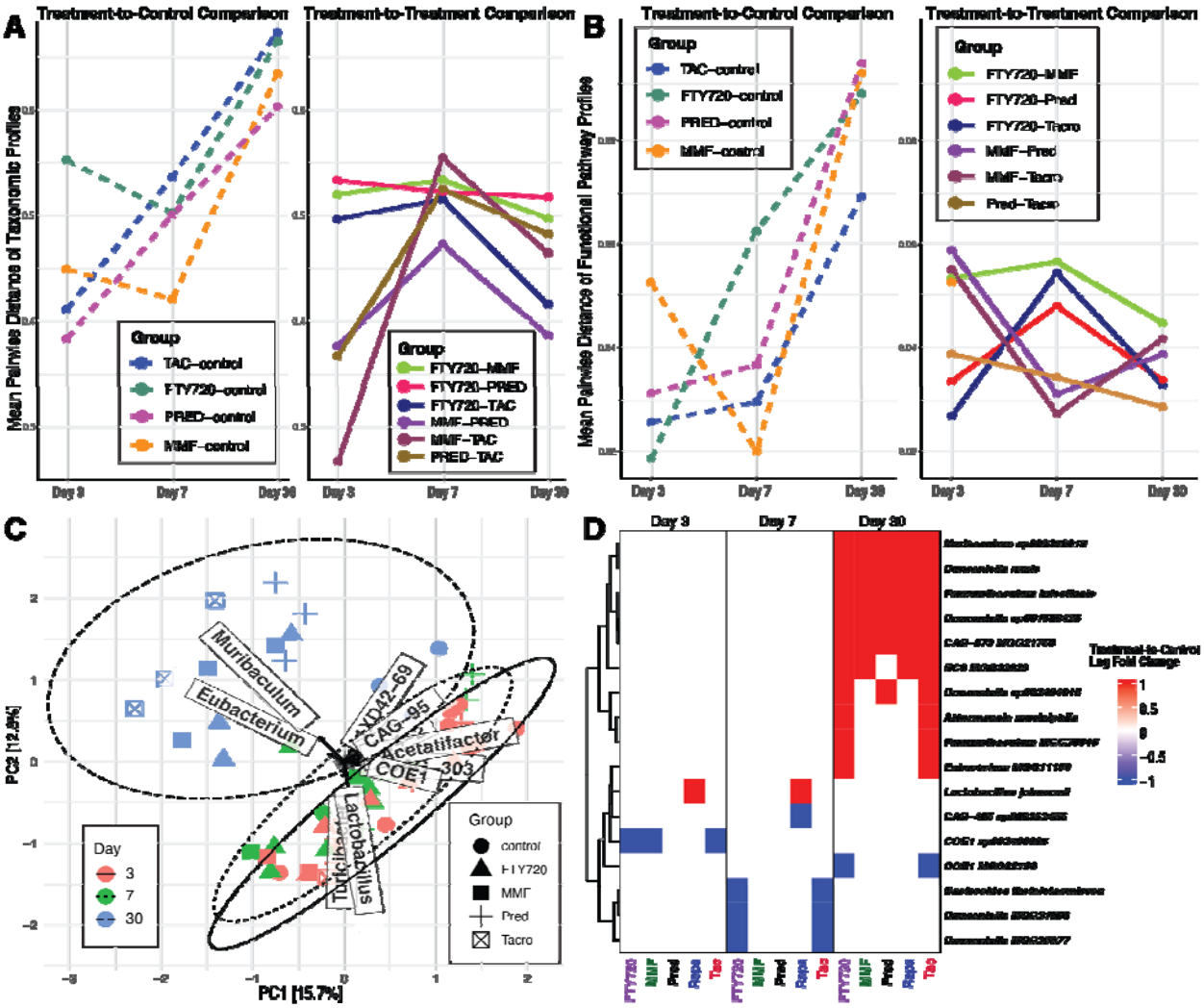

Figure 2.

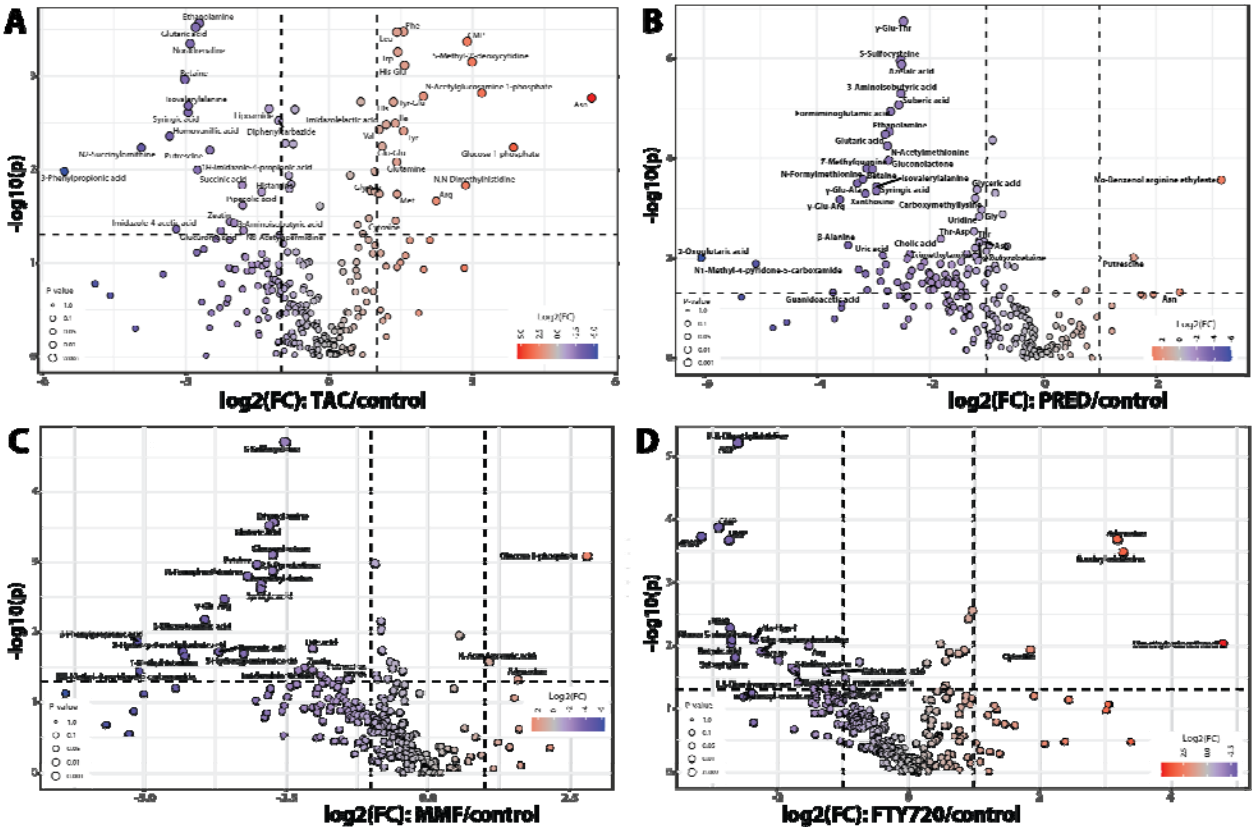
A
B
C
D
-log10(p)
log2(FC): TAC/control
log2(FC): PRED/control
log2(FC): MMF/control
log2(FC): FTY720/control
P value
Log2(FC)

Figure 3.

A)

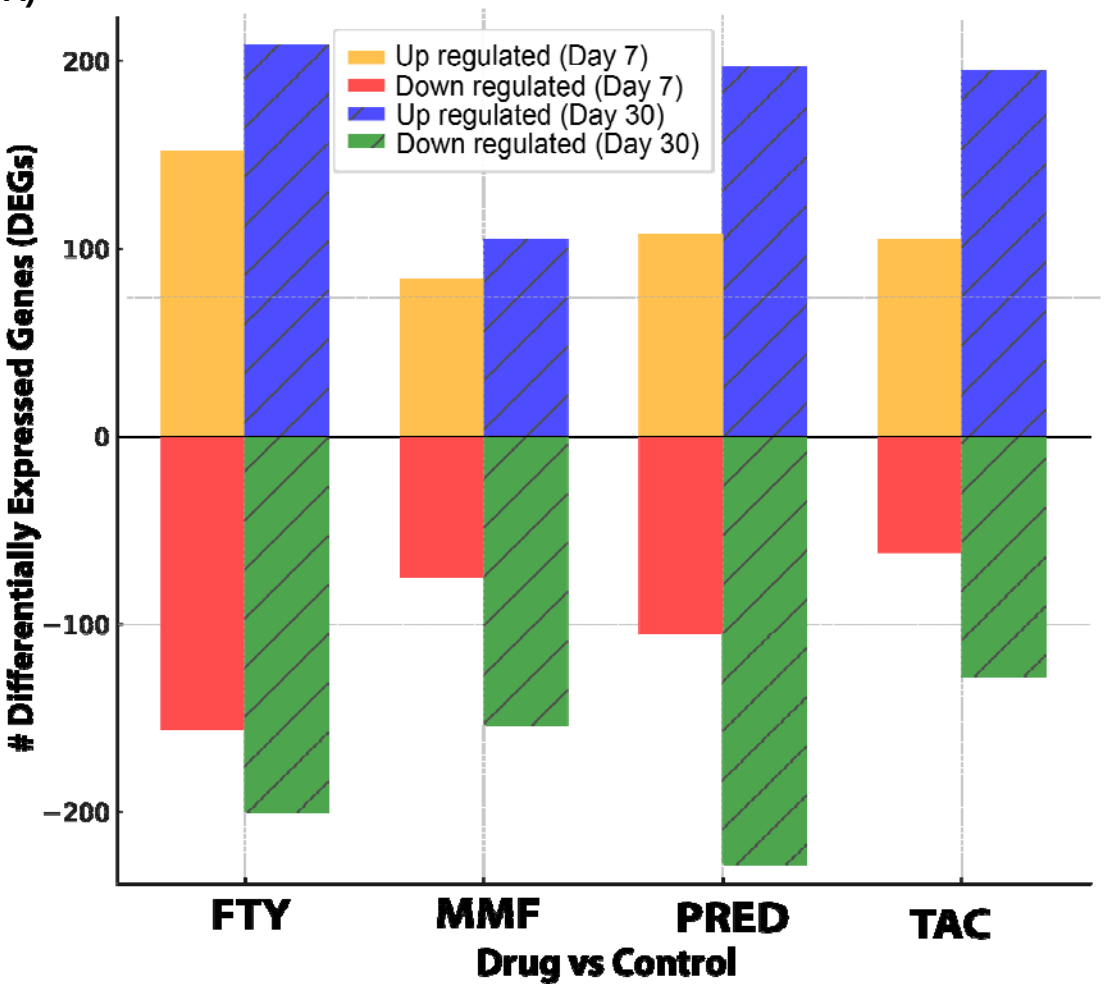
Up regulated (Day 7)
Down regulated (Day 7)
Up regulated (Day 30)
Down regulated (Day 30)
Differentially Expressed Genes (DEGs)
200
100
0
−100
−200
FTY
MMF
PRED
TAC
Drug vs Control

Figure 3.

B)

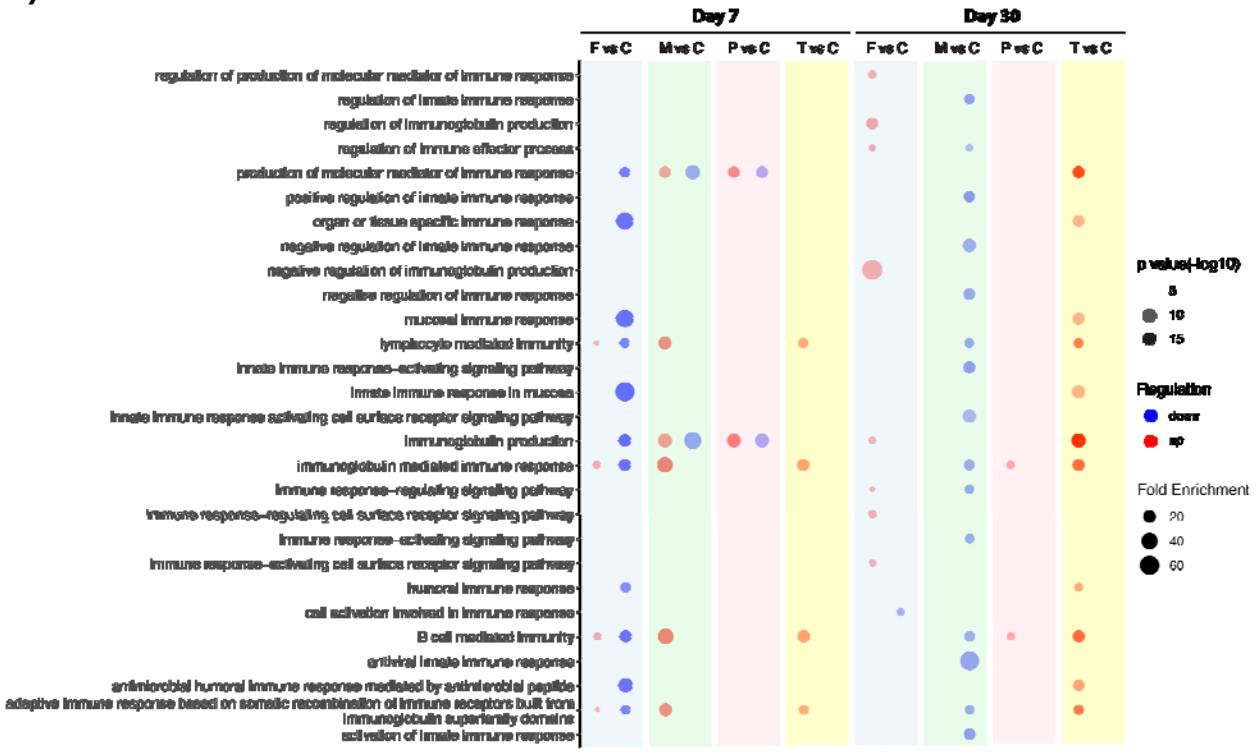
Day 7
Day 30
F vs C
M vs C
P vs C
T vs C
F vs C
M vs C
P vs C
T vs C
regulation of production of molecular mediator of immune response
regulation of innate immune response
regulation of immunoglobulin production
regulation of immune effector process
production of molecular mediator of immune response
positive regulation of innate immune response
organ or tissue specific immune response
negative regulation of innate immune response
negative regulation of immunoglobulin production
negative regulation of immune response
mucosal immune response
lymphocyte mediated immunity
innate immune response-activating signaling pathway
innate immune response in mucosa
innate immune response activating cell surface receptor signaling pathway
immunoglobulin production
immunoglobulin mediated immune response
immune response-regulating signaling pathway
immune response-regulating cell surface receptor signaling pathway
immune response-activating signaling pathway
immune response-activating cell surface receptor signaling pathway
humoral immune response
cell activation involved in immune response
B cell mediated immunity
antiviral innate immune response
antimicrobial humoral immune response mediated by antimicrobial peptide
adaptive immune response based on somatic recombination of immune receptors built from immunoglobulin superfamily domains
activation of innate immune response
p value(-log10)
5
10
15
Regulation
down
up
Fold Enrichment
20
40
60

Figure 4.

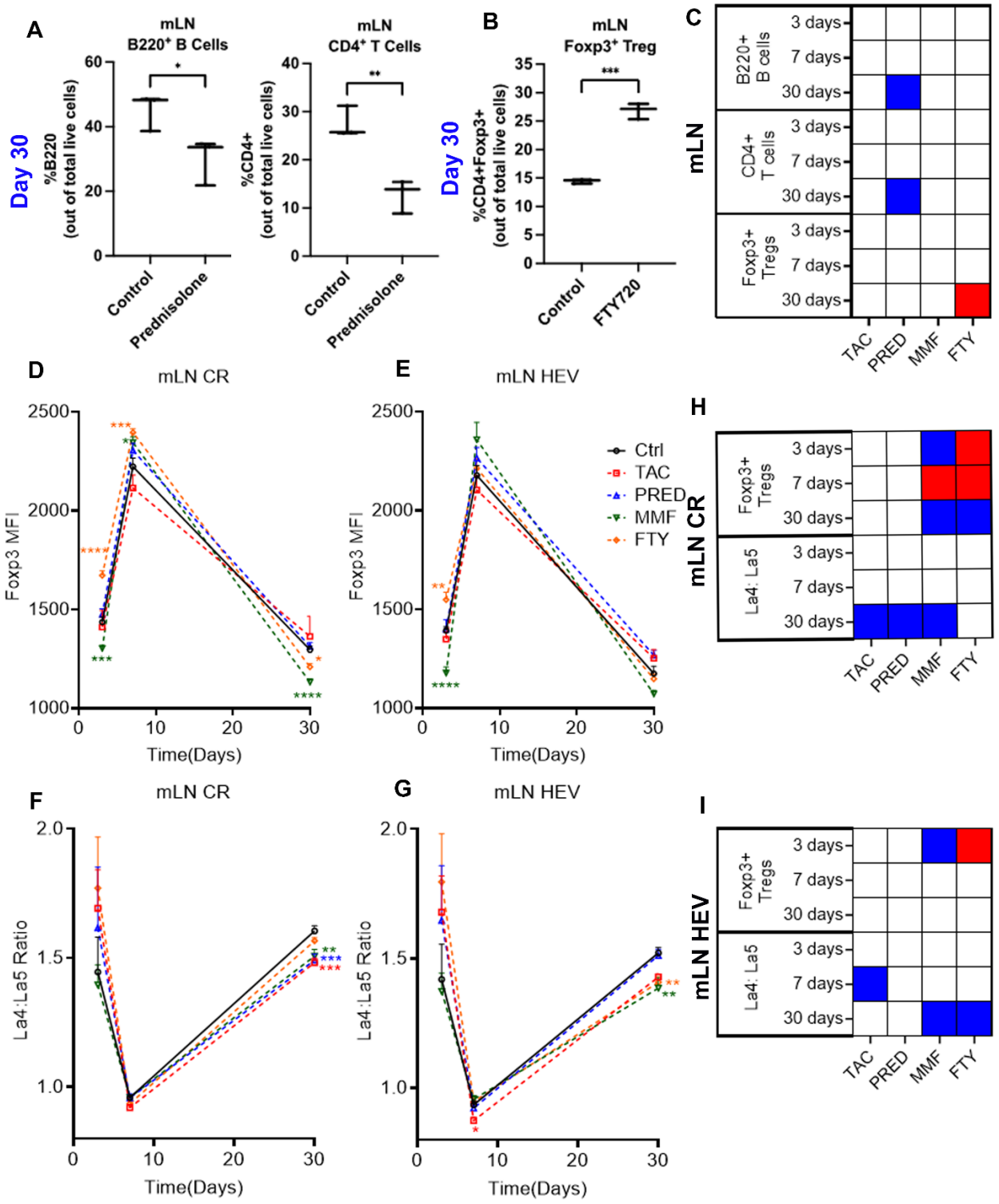
A
mLN
B220+ B Cells
Day 30
%B220
(out of total live cells)
Control
Prednisolone
mLN
CD4+ T Cells
%CD4+
(out of total live cells)
B
mLN
Foxp3+ Treg
Day 30
%CD4+Foxp3+
(out of total live cells)
FTY720
C
mLN
B220+ B cells
CD4+ T cells
Foxp3+ Tregs
3 days
7 days
30 days
TAC
PRED
MMF
FTY
D
mLN CR
Foxp3 MFI
Time(Days)
E
mLN HEV
Ctrl
TAC
PRED
MMF
FTY
H
mLN CR
Foxp3+ Tregs
La4: La5
I
mLN HEV
F
mLN CR
La4:La5 Ratio
G
mLN HEV

Figure 5.

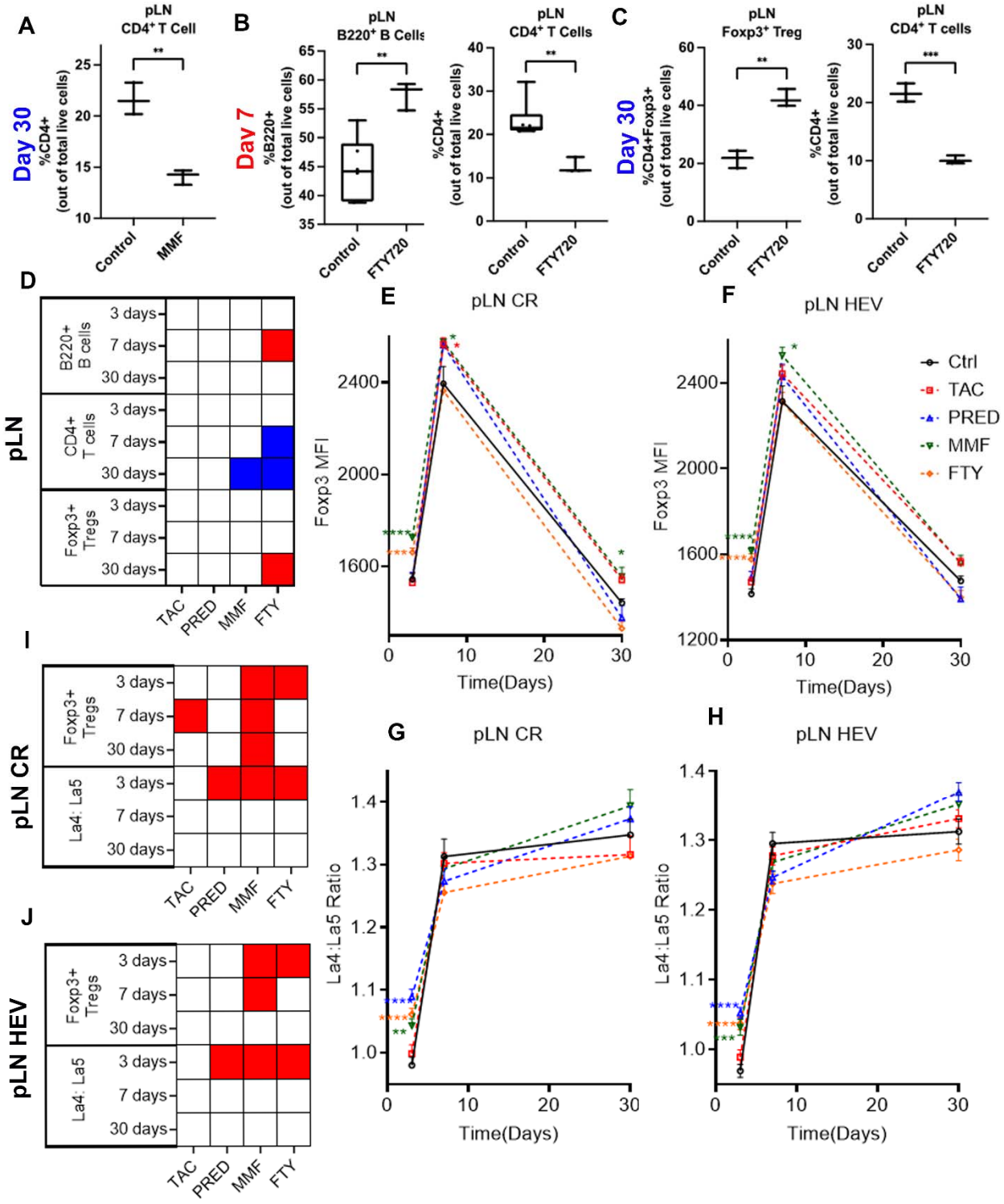
A
pLN
CD4+ T Cell
Day 30
%CD4+
(out of total live cells)
Control
MMF
B
pLN
B220+ B Cells
Day 7
%B220+
(out of total live cells)
Control
FTY720
pLN
CD4+ T Cells
%CD4+
(out of total live cells)
Control
FTY720
C
pLN
Foxp3+ Treg
Day 30
%CD4+Foxp3+
(out of total live cells)
Control
FTY720
pLN
CD4+ T cells
%CD4+
(out of total live cells)
Control
FTY720
D
pLN
B220+ B cells
CD4+ T cells
Foxp3+ Tregs
3 days
7 days
30 days
TAC
PRED
MMF
FTY
E
pLN CR
Foxp3 MFI
Time(Days)
F
pLN HEV
Foxp3 MFI
Time(Days)
Ctrl
TAC
PRED
MMF
FTY
I
pLN CR
Foxp3+ Tregs
La4: La5
3 days
7 days
30 days
TAC
PRED
MMF
FTY
G
pLN CR
La4:La5 Ratio
Time(Days)
H
pLN HEV
La4:La5 Ratio
Time(Days)
J
pLN HEV
Foxp3+ Tregs
La4: La5
3 days
7 days
30 days
TAC
PRED
MMF
FTY

Figure 6.

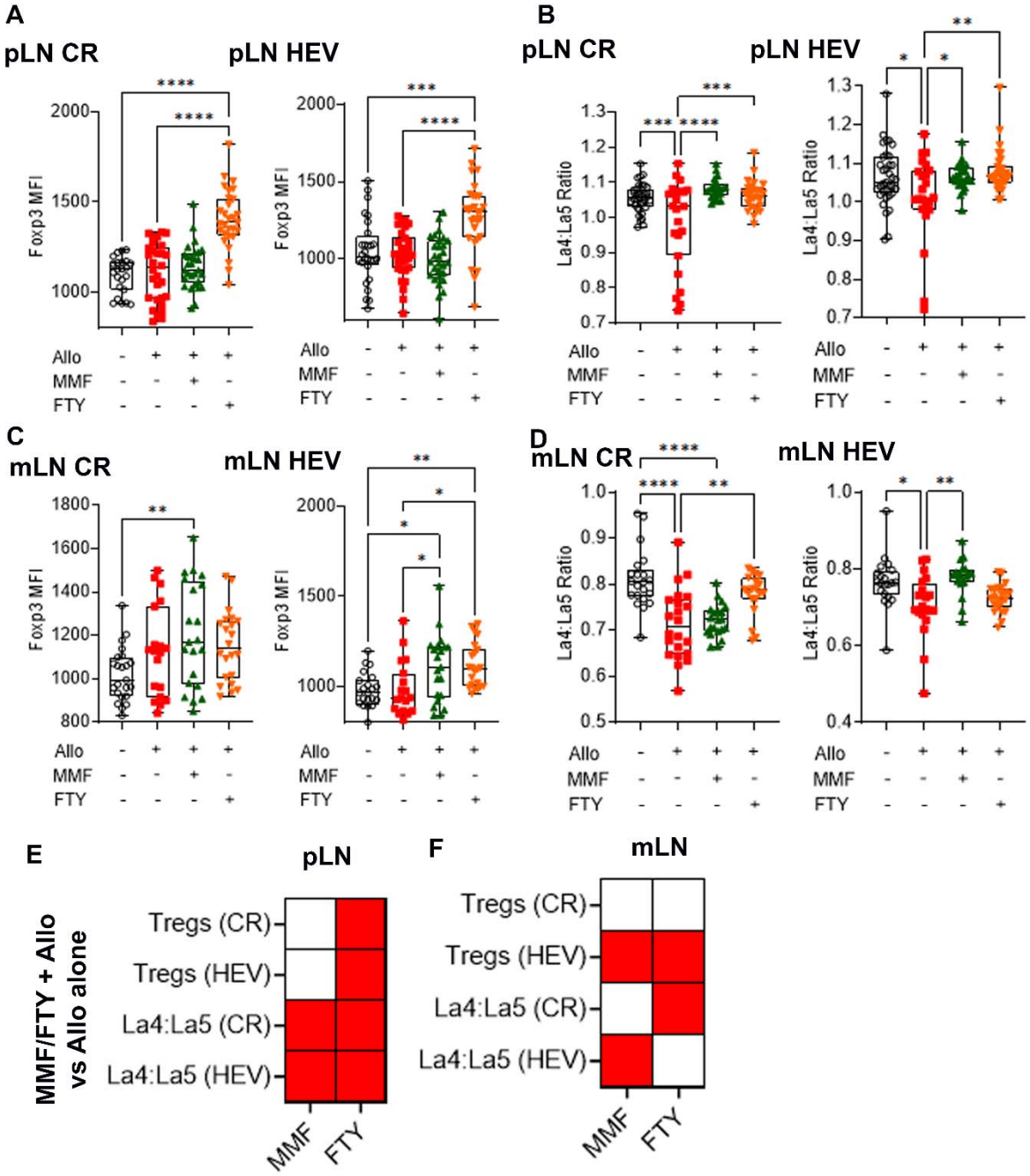
A
pLN CR
pLN HEV
Foxp3 MFI
Allo
MMF
FTY
B
pLN CR
pLN HEV
La4:La5 Ratio
C
mLN CR
mLN HEV
D
mLN CR
mLN HEV
E
pLN
MMF/FTY + Allo vs Allo alone
Tregs (CR)
Tregs (HEV)
La4:La5 (CR)
La4:La5 (HEV)
MMF
FTY
F
mLN

Figure 7.

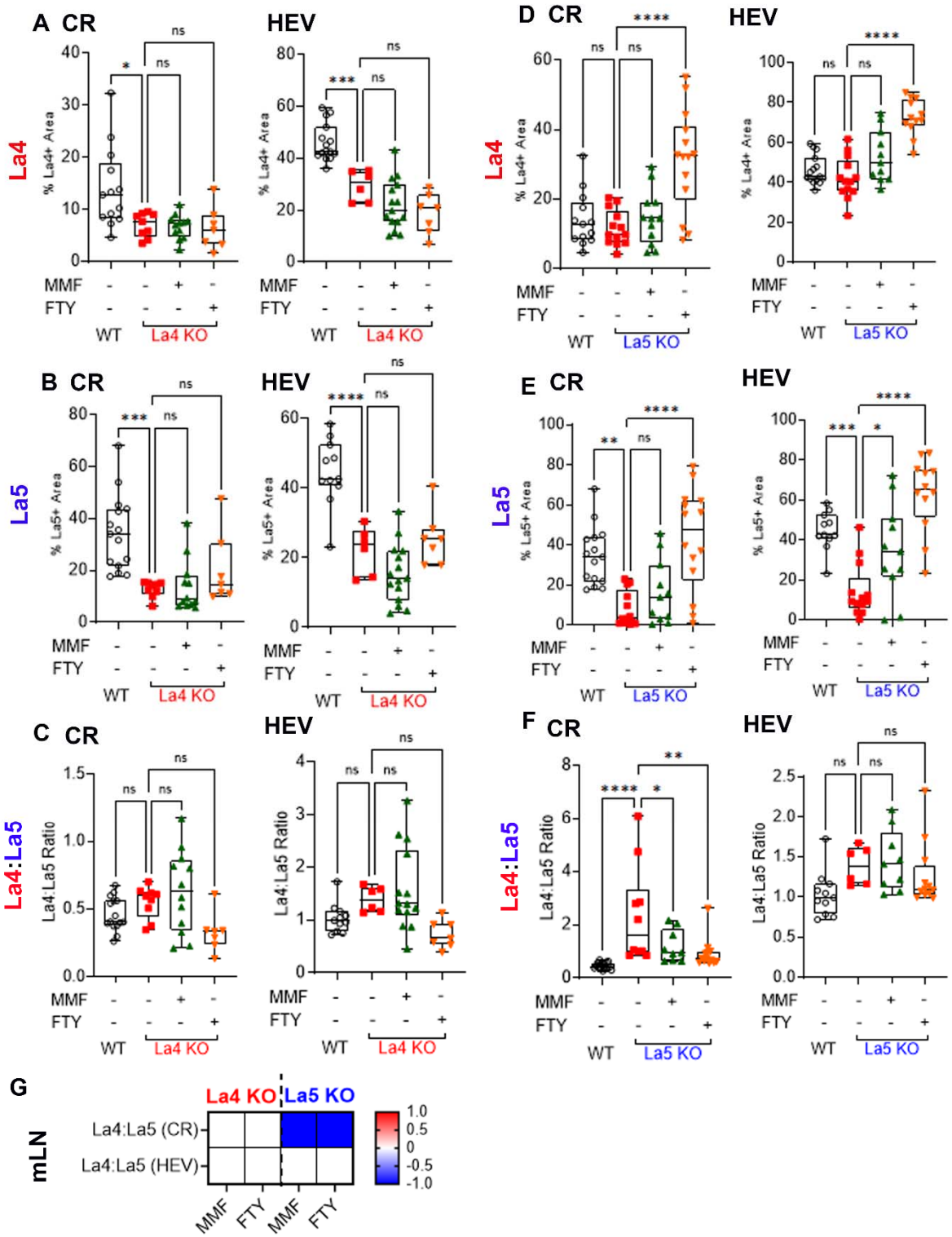
A CR
HEV
D CR
HEV
B CR
HEV
E CR
HEV
C CR
HEV
F CR
HEV
La4
La5
La4:La5
% La4+ Area
% La5+ Area
La4:La5 Ratio
MMF
FTY
WT
La4 KO
La5 KO
ns
G
mLN
La4 KO
La5 KO
La4:La5 (CR)
La4:La5 (HEV)
MMF
FTY
MMF
FTY
1.0
0.5
0
-0.5
-1.0

Figure 8.

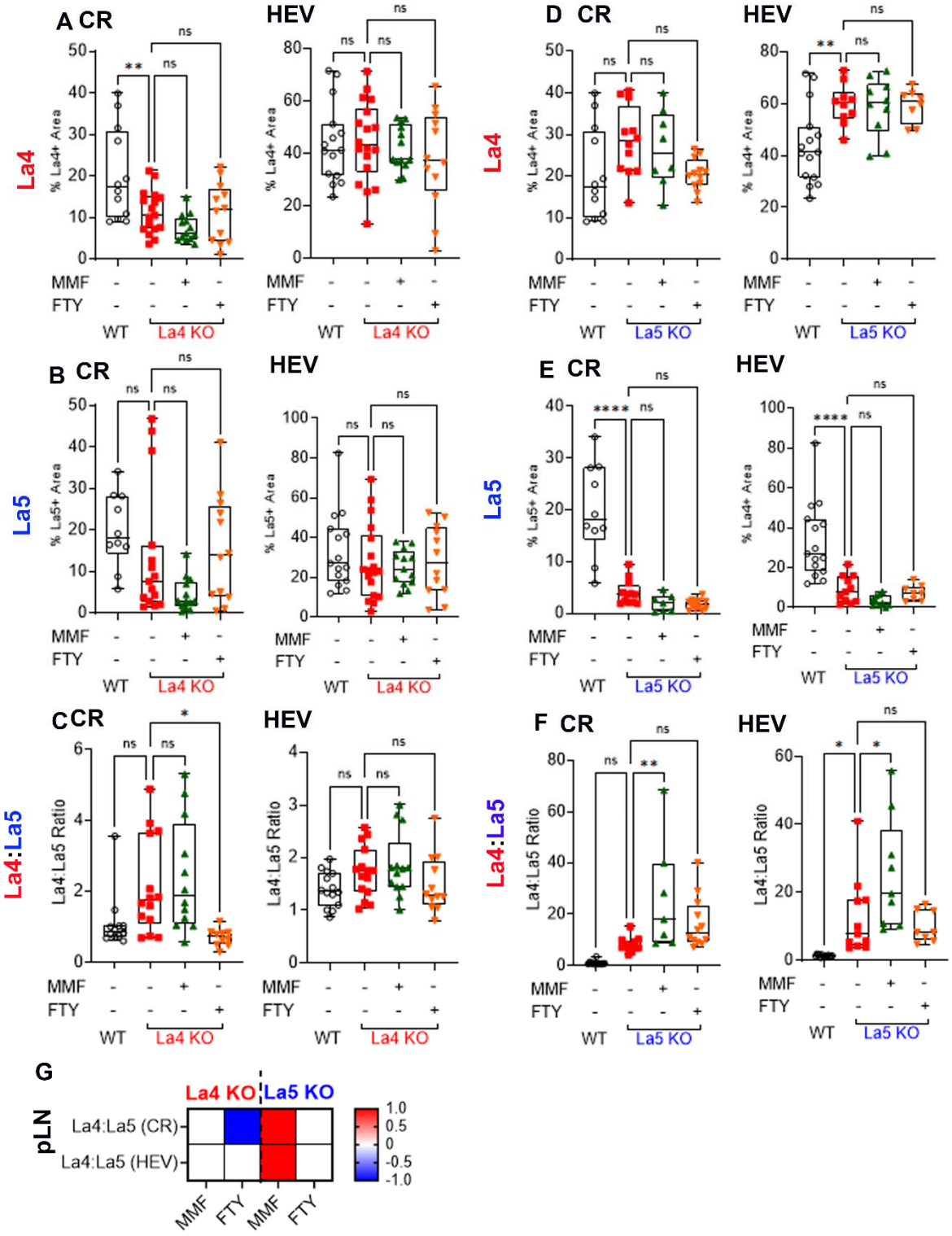
A CR
HEV
D CR
HEV
B CR
HEV
E CR
HEV
C CR
HEV
F CR
HEV
La4
La5
La4:La5
% La4+ Area
% La5+ Area
La4:La5 Ratio
MMF
FTY
WT
La4 KO
La5 KO
ns
G
La4 KO
La5 KO
pLN
La4:La5 (CR)
La4:La5 (HEV)
MMF
FTY
MMF
FTY
1.0
0.5
0
-0.5
-1.0